Journal of The
Electrochemical Society

Electrochemical Behavior and Self-Sealing Ability of Zirconium Conversion Coating Applied on Aluminum Alloy 3005 in 0.5 M NaCl Solution

To cite this article: Gavrilo Šekularac and Ingrid Milošev 2020 *J. Electrochem. Soc.* **167** 021509

Journal of The Electrochemical Society, 2020 **167** 021509

Electrochemical Behavior and Self-Sealing Ability of Zirconium Conversion Coating Applied on Aluminum Alloy 3005 in 0.5 M NaCl Solution

Gavrilo Šekularac[1,2] and Ingrid Milošev[1,*,z]

[1]*Jožef Stefan Institute, Department of Physical and Organic Chemistry, SI-1000 Ljubljana, Slovenia*
[2]*Jožef Stefan International Postgraduate School, SI-1000 Ljubljana, Slovenia*

Zirconium conversion coating (ZrCC) was prepared on aluminum-manganese alloy AA3005 by immersion in 200 ppm of H_2ZrF_6 bath for 10 min at room temperature. Potentiodynamic polarization curves and electrochemical impedance spectra were measured up to 10 and 40 days, respectively, in 0.5 M NaCl solution. Microstructural characterization of samples was carried out using scanning electron microscopy equipped with energy dispersive X-ray spectrometry, X-ray photoelectron spectroscopy, time-of-flight secondary ion mass spectrometry, focus ion beam microscopy and transmission electron microscopy. The coating had a tri-layer structure with a thickness of 200 nm in the proximity of intermetallic particles and 30 nm far from intermetallic particles at the coating matrix. Electrochemical measurements showed that the corrosion resistance of ZrCC on AA3005 was improving during immersion in NaCl solution, i.e., impedance value at low frequency increased with immersion time reaching the average value $8.5 \cdot 10^6\ \Omega{\cdot}cm^2$ at 3 mHz after 10 days immersion. Microstructural and compositional characterization showed that this behavior is related to the change in composition and structure of conversion coating including a transformation of ZrF_4/ZrO_xF_y to $ZrO_2 \cdot 2H_2O_{(s)}$ and formation of $Al(OH)_3$ in the top layer of ZrCC, respectively, accompanied by the change in thickness of individual layers within the coating.

 [DOI: 10.1149/1945-7111/ab6b0d]

Manuscript submitted October 30, 2019; revised manuscript received December 17, 2019. Published January 29, 2020.

Supplementary material for this article is available online

Chemical conversion coatings are formed by immersion, spraying, rinse or no-rinse process in which metal reacts with ions/substance from conversion bath forming an insoluble oxide-based coating at the surface of a metal.[1–5] They are usually inorganic in nature. The main purpose of these coatings is to improve the adhesion of organic paints and lacquer to the substrate; to facilitate adhesion, organic polymers and additives are often added.[1,6–12] Additionally, conversion coatings should improve the corrosion resistance of the substrate and the whole painted system.

For the last 100 years, state of the art conversion coatings were chromium conversion coatings (CCCs)[13,14] for aluminum/light metals and phosphate conversion coatings for ferrous metals.[15,16] As CCCs are nowadays being replaced due to carcinogenicity and toxicity of chromates, and phosphate conversion coatings are reconsidered due to environmental and economic issues, there is a great need to find a comparable, economical and green conversion processes. The most promising and already commercialized processes are the zirconium conversion coatings (ZrCCs), so-called Zirconization, and the trivalent chromium process (TCP).[1,2,17] Zirconization has developed very quickly since the first patents /pioneering scientific work in the early 1990s,[6,18–21] followed by the 1st generation ZrCCs in 2002[22,23] and 2nd generation in 2010.[24,25] The ZrCC process operates at room temperature, there is minimal waste disposal, rinsing water can be recirculated and the control of bath parameters is simple.[26,27] The main advantage of the ZrCC process is that it can be applied to almost all metals, so is a "multi-metal process." In defense and aerospace industries, the TCP process is a preferable choice over the ZrCC due to its better corrosion resistance. TCP coating is basically ZrCC with embedded Cr^{3+} ions as an active corrosion protection agent.[2,17,28,29] Due to indirect hazards related to resources, extraction, disposal of Cr^{3+} ions and new evidence that even Cr^{3+} ions can also cause genotoxicity and cancer in humans, it could be forbidden in the future.[14,30,31] So there is a great need in the industry to develop a completely Cr-free process with corrosion performance at the level of CCCs.

The formation of ZrCC is an electrochemical driven process by a difference of Volta potential between intermetallic particles (IMPs) and Al matrix.[11,32,33] It starts by thinning of a native protective oxide layers and activation of the surface. At the same time, the oxygen reduction reaction and hydrogen evolution reactions take place at exposed IMPs causing a local alkalization that establishes the conditions for precipitation of zirconium oxide/hydroxide. After the coating covers the IMPs, it starts to growth laterally covering the whole surface. Due to the nature of this process, conversion coating is much thicker at/in the proximity of IMPs.[32]

There have been many studies of ZrCC on aluminum alloys,[6,8,11,19,32–48] magnesium alloys,[49,50] zinc,[51–54] steel.[10,55–60] Addition of a small amount of Cu speeds up the conversion process and produces thicker coating,[39,54,61] while addition of a small amount of Si can also produce thicker conversion coatings.[44] Surface pre-conditioning has an important role in the microstructure and properties of ZrCCs.[40,41,43] Additionally, surface pre-treatment influences acid-base properties and the amount of OH^- groups in the final ZrCC.[47,51,52] Coating thickness increases with the agitation of the bath by factor 2–4 depending on the substrate.[42] ZrCCs are usually 30–80 nm and were reported to exhibit a bi- or even tri-layer structure.[46] ZrCCs improve adhesion of top organic coats, reduce the rate of cathodic delamination and improve corrosion resistance on different substrates.[7,59,62–65] Addition of corrosion inhibitors such as Ce, V, Mo into ZrCC can provide a certain degree of active corrosion protection to these coatings.[35,37,38]

Aluminum-manganese alloy AA3005 has good workability, medium strength, good electrical and thermal conductivity and excellent corrosion resistance. It is used as a heat exchanger in automotive and other industries, in architectural industries, for brazing and cladding, etc. There have been several studies on the nature and stability of Al_2O_3 formed on 3*xxx* alloys,[66–68] but only a few studies about conversion pre-treatment of this alloy. Smit et al. studied no-rinse pre-treatment of AA3003 in conversion bath containing 0.1 M solution of H_2TiF_6.[9,69] When coated with titanium conversion coating the corrosion resistance in NaCl was initially not so good but it improved with immersion time. TEM images showed that the coating was 30 nm thick.[69] Thermal treatment had a beneficial effect on the corrosion properties of H_2TiF_6-pre-treated

*Electrochemical Society Member.
[z]E-mail: ingrid.milosev@ijs.si

AA3003.[70] Banczek et al. studied Ce conversion coatings on AA3003 and compared it with a commercial TCP conversion coating (SurTec 650 Chromital).[71]

Therefore, there is a lack of studies about zirconium conversion coatings applied to AA3*xxx* alloys. Moreover, the extraordinary behavior of titanium conversion coating on AA3003 which improved with time, as noticed by Smit et al.[69] deserves further mechanistic understanding. In our previous study, the commercial TCP coating SurTec®650 containing Cr(III) and Zr deposited on AA3003 was studied.[72] This commercial coating exhibited good corrosion resistance in simulated acid rain and sodium chloride solution but only after longer immersion in solution, i.e., 24 h. This interesting behavior is studied in more detail in this study devoted to Zr-based coatings only deposited over AA3005. The electrochemical behavior of ZrCCs prepared by immersion of AA3005 in the conversion bath of hexafluorozirconic acid (H_2ZrF_6) was investigated.

Microstructural characterization of the coated substrate was carried out using scanning electrochemical microscopy equipped with energy X-ray dispersive spectrometer (SEM/EDS), cross section focus ion beam microscopy (FIB), transmission electron microscopy (TEM), X-ray photoelectron spectroscopy (XPS) and time-of-flight secondary ion mass spectrometry (ToF-SIMS). Electrochemical characterization of samples was carried out in a 0.5 M NaCl solution by measuring open circuit potential (OCP) vs time curves, potentiodynamic polarization curves and electrochemical impedance spectra. Special attention was devoted to the long-term corrosion resistance in NaCl, up to 40 days. An interesting behavior of improvement of corrosion characteristics of coated samples with time was confirmed. Based on the results obtained we were able to address this phenomenon and postulate the mechanism of self-sealing or active protection of Zr-conversion coatings on Al-Mn alloy AA3005.

Experimental

Materials, sample preparation and chemicals.—Aluminum alloy AA3005 / UNS-A93005 (Mn 1–1.5 wt%, Mg 0.2–0.6 wt%, Fe 0–0.7 wt%, Si 0–0.6 wt%, Cu 0–0.3, Zn 0–0.25 wt%, Cr 0–0.1 wt %, Ti 0–0.1 wt%, residuals 0.15 wt%) in form of foil (thickness 70 microns) produced by Impol 2000 d.d. (Slovenska Bistrica, Slovenia) was used as a substrate. The composition given was provided by the supplier. Samples used in experiments were cut in a rectangular shape with dimensions of 3 cm × 3 cm.

The following chemicals were used for experiments: NaCl (for analysis, Fischer Scientific, Leicestershire), H_2ZrF_6 (50 wt% in water, Sigma-Aldrich, Saint Louis, USA), NH_4HCO_3 (reagent grade, Sigma-Aldrich, Steinheim, Germany) and Metaclean® (alkaline cleaner, Amity international, Barnsly, United Kingdom). Milli-Q Direct water with the resistivity of 18.2 MΩ·cm at 25 °C (Merck, Darmstadt, Germany) was used for rinsing and for solution preparation.

pH was measured using pH meter 827 pH-lab equipped with Unitrode/Pt1000 (Metrohm AG, Herisau, Switzerland). Teflon beakers (V = 1 L) were used for conversion baths, while glass beakers (V = 600 ml) were used for alkaline cleaner and rinsing baths. Sample holders were made of teflon and conversion coating solutions were stored in polyethylene bottles.

Preparation of conversion coatings.—Conversion bath contained $1{\cdot}10^{-3}$ mol L^{-1} (200 ppm) of H_2ZrF_6 and pH was set to 4.8 using 15 wt.% NH_4HCO_3. The conversion was carried out at room temperature.

Samples were chemically cleaned by immersion in 5 wt.% Metaclean solution (T = 57 °C, stirring rate 150 rpm) for 3 min. Immediately afterward, samples were washed off with Milli-Q Direct water and then rinsed by dipping in Milli-Q Direct water bath for 45 s. Immediately afterward, the sample was dipped in a conversion coating bath (T = 25 °C, stirring rate 450 rpm) for 10 min. Immediately afterwards the sample was rinsed with Milli-Q Direct water and washed off by dipping it in Milli-Q Direct water bath for 1 min. The sample was then dried with N_2 stream and left to dry in air for 24 h.

As-received (bare) samples refer to AA3005 used in as-received conditions without any chemical cleaning.

Electrochemical characterization.—Electrochemical experiments were carried out with a Multi Autolab/M204 (Metrohm Autolab, Utrecht, Netherlands) potentiostat/galvanostat controlled by Nova 2.1 software. Electrochemical measurements were repeated for each condition for at least three different samples. Representative measurements are presented in plots and average values together with standard deviation in tables. Measurements were conducted in a standard three-electrode flat cell with a volume of 250 mL. The sample was the working electrode, a carbon rod was the counter electrode, and a saturated $Ag/AgCl_{(sat)}$ electrode was the reference electrode (E_{SHE} = 0.198 V). All potentials in the text refer to the $Ag/AgCl_{(sat)}$ scale. The electrolyte was freshly prepared 0.5 M NaCl.

Prior to electrochemical measurement samples were allowed to rest at open circuit potential (OCP) for 5 min, 1 h, 2 h, 1 day, 2 days, 3 days, 4 days, 5 days and 10 days.

Electrochemical measurements were conducted in the following sequence from least destructive to more destructive: (i) measurement of the (OCP) as a function of time during for 5 min, (ii) recording of linear polarization curves, and (iii) recording of potentiodynamic polarization curves. The system was allowed to rest for 10 s before switching to the next electrochemical technique.

Linear polarization curves (LPR) were run in the range from—10 to 10 mV vs OCP using a 0.1 mV s^{-1} scan rate. Polarization resistance ($R_{p,\ LPR}$) was determined as the slope of the fitted potential (E) vs current density (j) curve using Nova 2.1 software.

Potentiodynamic polarization curves measurements were made in the potential region starting from −250 mV vs OCP in the anodic direction until current reached 0.1 mA. The scan rate was 1 mV s^{-1}.

Corrosion current density and corrosion potentials were determined using Nova 2.1 software based on the Tafel extrapolation method.[73] Polarization resistance was calculated also from parameters obtained by Tafel extrapolation ($R_{p,\ Tafel}$) method using Nova 2.1 software based on Eq. 1 in accordance with standard ASTM G59–97.[74]

$$R_{p,Tafel} = \frac{B}{j_{corr}} \quad [1]$$

where B is the Stern-Geary constant.

Electrochemical impedance spectroscopy (EIS) spectra were recorded from 100 kHz to 3 mHz frequency using an AC potential amplitude of 10 mV. Spectra were recorded at the OCP, periodically every day up to 40 days of immersion or until the samples were pitted.

Microstructural characterization.—Surface characterization was performed using scanning electron microscopy combined with energy dispersive X-ray spectrometry (SEM/EDS), focused ion beam microscopy (FIB) equipped with EDS, transmission electron microscopy (TEM) and X-ray photoelectron spectroscopy (XPS).

SEM images were taken in secondary electron (SE) and back-scattered electron (BSE) modes using a FEI Helios Nanolab 650 microscope. EDS spectra were taken using an Oxford Instruments AZtec system with X-max SDD (50 mm^2) detector. The analysed area was 100 nm^2 with an analysis depth of 100 nm (near surface condition) at 3 kV beam energy, to few micrometers in diameter and the analysed depth around 1 μm for higher beam energies. EDS mapping was recorded with 3 kV beam energy and resolution of 1024 lines. Prior to analysis, samples were coated with a thin carbon layer to reduce the charging effect.

FIB was used to analyse the cross-section of conversion coatings. A FEI Helios Nanolab 650, equipped with EDS, was first used to

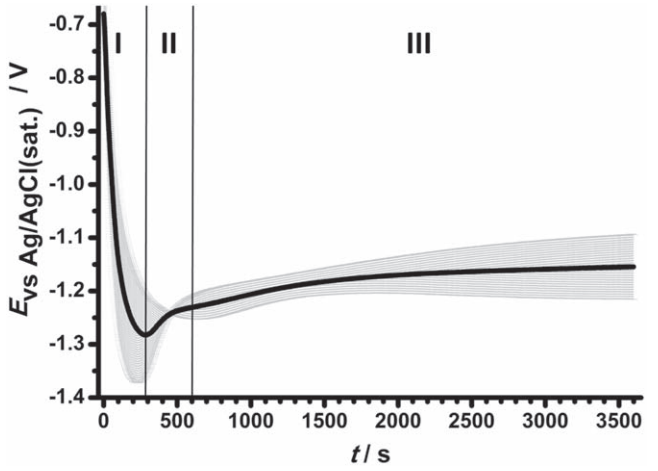

Figure 1. Open circuit potential measurement during the formation of zirconium conversion coating on AA3005 in $1 \cdot 10^{-3}$ M H_2ZrF_6 conversion bath. Average value of 3 repetitions on different samples is presented by solid curve and standard deviation as grey area. Numerals I, II and III denote the regions of surface activation, initial coating formation and growth, respectively.

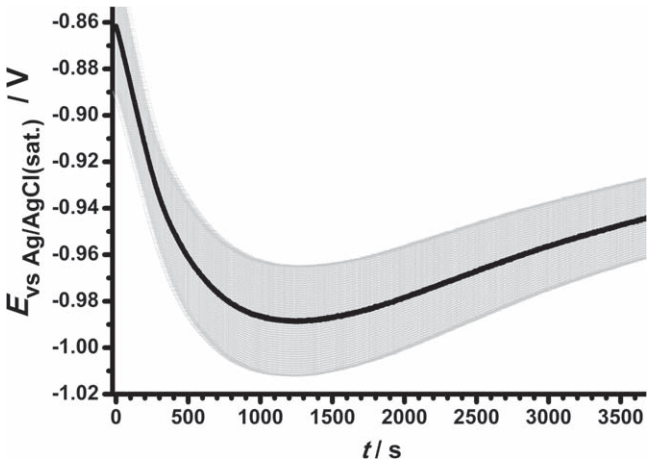

Figure 2. Open circuit potential during the first 2 h after immersion of zirconium conversion coated AA3005 samples in 0.5 M NaCl. Average value of 4 repetitions on different samples is presented by solid curve and standard deviation as grey area.

deposit a 1 μm thick Pt protection layer. Then, a relatively large cross-section was made by a rough removal of material with Ga ions (30 keV/48 nA) followed by a rough polishing (30 keV/22 nA) and a fine polishing (30 keV/9 nA). EDS maps of the cross-section were recorded with a resolution of 1024 lines. The average thickness of oxide layers was evaluated using ImageJ programme.

TEM was used to analyse the cross section of the conversion coatings and assess its thickness, composition and structure. Detailed structural investigations of the sample were performed using a conventional 200 kV transmission electron microscope (JEM-2010F, Jeol Ltd., Tokyo, Japan). Chemical analysis was performed using a Si(Li) EDS detector.

For TEM cross-section analysis, the sample was mounted and fitted into 3 mm brass cylinders using epoxy glue between two silicon blocks on each side to improve strength. The TEM specimen was ground to a thickness of 100 μm and dimpled down to 15 μm at the disc center (Dimple grinder, Gatan Inc., Warrendale PA, USA). The TEM specimen was finally ion-milled (PIPS, Precision Ion Polishing System, Gatan Inc., USA) using 3 kV Ar^+ ions at an incidence angle of 8° until perforation.

XPS was carried out using a PHI-TFA XPS spectrometer (Physical Electronic Inc.). The vacuum during the XPS analysis was in the range of 10^{-9} mbar. The analysed area was 0.4 mm in diameter and the depth about 3–5 nm. X-rays were provided from a monochromatic Al Kα source at a photon energy of 1486.6 eV. XPS spectra were analysed by Multipack software, version 8.0 (Physical Electronics Inc.). Spectra were calibrated relative to the position of C 1 s peak at 284.8 eV.

ToF-SIMS ion depth profiles were made using a ToF-SIMS V spectrometer (ION TOF GmbH—Munster, Germany). The analysis chamber was operated at a pressure below $\sim 10^{-9}$ mbar. Ion depth profiles for positive ions were recorded by interlacing a pulsed 30 keV Bi^+ primary ion source delivering 1 pA of target current over a 100 × 100 μm^2 area with sputtering using a 2 keV O_2 source beam delivering 544 nA of target current over a 400 × 400 μm^2 area. Depth profiles for negative ions were recorded by interlacing a pulsed 30 keV Bi^+ primary ion source delivering 1.2 pA of target current over a 100 × 100 μm^2 area with sputtering using a 2 keV Cs^+ source beam delivering 523 nA of target current over a 400 × 400 μm^2 area.

Results and Discussion

OCP measurements during the formation of conversion coating.—OCP during coating formation was measured in order to follow the kinetics of conversion coating formation and to determine when the formation of the coating was completed. OCP curves measured during immersion in the H_2ZrF_6 conversion bath are presented in Fig. 1. The formation of the coating from the conversion bath can be described with the following steps.[1,32,44] Activation of the surface caused by the initial attack of aggressive ZrF_6^{2-} ions leads to the dissolution of naturally formed aluminum oxide layer Al_2O_3 (Eq. 2) that corresponds to decay of OCP (Fig. 1, region I). At the same time, oxygen reduction and hydrogen evolution reactions take place at cathodic sites and lead to local alkalization up to pH = 8.5 near cathodic sites (Eqs. 3 and 4).[45] This establishes the conditions for the initiation of coating formation (Eq. 5). At the OCP minimum the processes of natural oxide dissolution and conversion coating formation are in equilibrium. Region II, denoted by the progressive shift in OCP to more positive values, marks an increased growth of conversion coating over film dissolution. In this region, the formation and growth of conversion coating in the form of zirconium oxide/zirconium oxyfluoride takes place caused by the increased value of pH.

$$Al^{3+}_{(aq)} + ZrF_6^{2-}{}_{(aq)} \rightarrow AlF_6^{3-}{}_{(aq)} + Zr^{4+}{}_{(aq)} \quad [2]$$

$$O_{2(g)} + 2H_2O + 4e^- \rightarrow 4OH^-{}_{(aq)} \quad [3]$$

$$2H^+{}_{(aq)} + 2e^- \rightarrow H_{2(g)} \quad [4]$$

$$ZrF_6^{2-}{}_{(aq)} + 4OH^-{}_{(aq)} \rightarrow ZrO_2 \cdot 2H_2O_{(s)} + 6F^-{}_{(aq)} \quad [5]$$

At the end of region II, the OCP again makes an inflection point indicating that a steady state deposition process is reached. This point denotes the beginning of region III. At longer conversion times the conversion coating still continues to grow but due to thickness increase the cracking of the coating occurs and it loses its protective ability.[54,75–77] Based on the OCP measurements during ZrCC formation we conclude that the coating formation was completed after 10 min. This conversion time was then taken for the preparation of ZrCCs for all further experiments.

Open circuit potential during immersion of conversion coatings in 0.5 M NaCl.—Within the first 1000 s to 1200 s after immersion of conversion coated AA3005 sample in 0.5 M NaCl, the OCP decreases rapidly (Fig. 2). This indicates the initial dissolution of the conversion coating in chloride containing solution and

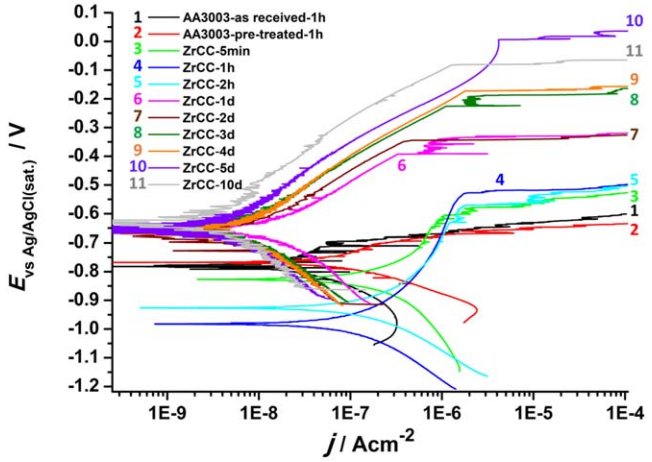

Figure 3. Potentiodynamic polarization curves recorded in 0.5 M NaCl for as-received (bare), chemically pre-treated and zirconium conversion coated AA3005. As-received and chemically pre-treated samples were stabilized for 1 h at the OCP prior measurement; conversion coated samples were stabilized for different periods of time (from 5 min up to 10 days). Electrochemical data deduced from polarization curves are given in Table I.

penetration of electrolyte through the conversion coating to the substrate and intermetallic particles (IMPs). After that period, the OCP started to recover and during the next 6000 s shifted towards more positive values, indicating a progressive recovery or sealing of conversion coatings.[78] This is a first order approximation of potential active corrosion protection, which is further examined in the following experiments.

Electrochemical potentiodynamic characterization.— Potentiodynamic polarization curves were recorded for as-received (bare), chemically pre-treated and conversion coated AA3005 samples to evaluate the performance of conversion coatings (Fig. 3, Table I). Bare and chemically cleaned samples were allowed to stabilize for 1 h at the OCP prior to electrochemical measurements, whereas for the conversion coated samples the immersion (stabilization) times at the OCP were up to 10 days.

Polarization curves for bare and chemically pre-treated samples are typical for aluminum alloys in chloride solution with cathodic process related to oxygen reduction and anodic process related to the dissolution of aluminum oxide and localized corrosion at the IMPs.[79] Prior to breakdown at the pitting potential (E_{pit}), the AA3005 alloy exhibits a passivity region ($\Delta E = |E_{pit}\text{-}E_{corr}|$) of approximately 100–150 mV indicating that it is quite resistant in chloride environment, especially compared to for example copper- or zinc-containing Al alloys.[80] Chemically pre-treated AA3005 exhibited 2-times larger corrosion current density and reduced ΔE in comparison with bare AA3005 sample (Fig. 3, Table I). Chemical pre-treatment cleaned and activated the surface of AA3005 for the conversion process by removing organic contaminants and natural aluminum oxide from alloy surface thus resulting in larger current densities.

After 1 h of immersion in 0.5 M NaCl solution, both bare AA3005 and chemically pre-treated AA3005 exhibited smaller j_{corr} and narrower ΔE window in comparison with conversion coated samples measured after 5 min, 1 h and 2 h immersion in 0.5 M NaCl. These results indicate that the conversion coating process did not provide—significant protection to AA3005. In order to monitor and evaluate corrosion behavior further, conversion coated AA3005 samples were immersed for longer times prior to electrochemical measurements, i.e. up to 10 days. Please note that data on all repetitions and electrochemical parameters deduced are presented in Supplement material (Figs. SI–S3, Table SI are available online at stacks.iop.org/JES/167/021509/mmedia).

With the prolongation of immersion time above 1 h, the j_{corr} of ZrCC samples progressively decreased, E_{corr} shifted more positive and ΔE increased. After 24 h h of immersion, the j_{corr} was smaller by 1 order of magnitude, while OCP was shifted towards more positive values reaching −0.71 V. This was a significant improvement in the performance of ZrCC compared to the short immersion

Table I. Electrochemical data deduced from potentiodynamic polarization measurements for as-received, chemically pre-treated and zirconium conversion coated AA3005 exposed to 0.5 M NaCl for different periods of time prior to electrochemical measurement. In table, average values and standard deviation (SD) are given obtained on different samples.

Sample	Jcorr A cm^{-2}	OCP V	Ecorr V	Epit V	ΔE[a)] V	βa mV/dec	βc mV/dec	$R_{P,LPR}$ Ω cm^2	$R_{P,Tafel}$ Ω cm^2
As-received-1h	3.9E-08	−0.83	−0.82	−0.67	0.15	220	116	8.6E + 05	9.3E + 05
+SD	1.1E-08	0.02	0.03	0.03	0.04	23	19	1.5E + 05	3.2E + 05
Pre-treated-1h	7.5E-08	−0.74	−0.78	−0.68	0.10	176	102	4.6E + 05	3.8E + 05
SD	1.2E-08	0.01	0.01	0.02	0.02	44	4	2.0E + 05	4.4E + 04
ZrCC-5 min	2.4E-07	−0.87	−0.83	−0.61	0.22	367	320	1.8E + 05	3.0E + 05
SD	4.5E-08	0.02	0.03	0.02	0.02	72	43	1.3E + 04	3.0E + 04
ZrCC-1h	2.3E-07	−0.93	−0.94	−0.63	0.31	416	177	2.6E + 05	2.4E + 05
SD	4.4E-08	0.01	0.03	0.02	0.02	56	30	3.3E + 04	3.7E + 04
ZrCC-2h	1.6E-07	−0.89	−0.90	−0.59	0.34	285	194	3.6E + 05	3.1E + 05
SD	1.1E-08	0.02	0.02	0.01	0.04	28	9	6.7E + 04	3.5E + 04
ZrCC-1d	1.4E-08	−0.71	−0.70	−0.40	0.29	150	188	2.8E + 06	3.2E + 06
SD	8.1E-09	0.02	0.02	0.12	0.11	50	64	1.2E + 06	1.2E + 06
ZrCC-2d	8.0E-09	−0.69	−0.69	−0.36	0.33	176	188	3.0E + 06	5.4E + 06
SD	3.5E-09	0.03	0.03	0.11	0.11	26	44	1.5E + 06	1.4E + 06
ZrCC-3d	6.9E-09	−0.69	−0.68	−0.25	0.43	209	189	5.8E + 06	6.7E + 06
SD	2.6E-09	0.03	0.03	0.09	0.09	46	29	5.6E + 06	1.5E + 06
ZrCC-4d	5.5E-09	−0.67	−0.67	−0.32	0.35	203	197	4.1E + 06	9.1E + 06
SD	2.1E-09	0.03	0.04	0.10	0.12	23	27	2.8E + 06	3.5E + 06
ZrCC-5d	5.1E-09	−0.66	−0.67	−0.17	0.49	220	184	4.0E + 06	9.6E + 06
SD	2.0E-09	0.03	0.04	0.20	0.20	55	41	3.4E + 06	3.2E + 06
ZrCC-10d	3.2E-09	−0.65	−0.67	−0.22	0.45	235	173	5.3E + 06	1.6E + 07
SD	1.8E-09	0.03	0.04	0.13	0.09	29	54	5.0E + 06	5.1E + 06

a) $\Delta E = |E_{pit}\text{-}E_{corr}|$.

of 1 h. The trend of decreasing corrosion current densities continued up to 10 days of immersion in 0.5 M NaCl solution reaching OCP of −0.65 V, j_{corr} of $3{\cdot}10^{-9}$ A·cm^{-2}, and ΔE of 0.45 V. This electrochemical behavior indicates that ZrCC on AA3005 acts as an anodic inhibitor and that some kind of self-sealing/active corrosion protection takes place during prolonged immersion in 0.5 M NaCl.

Electrochemical impedance spectroscopy.—To evaluate the performance of conversion coatings the electrochemical impedance spectra (EIS) were measured at OCP for as-received, chemically pre-treated and ZrCC coated AA3005 samples until pitting occurred. Curves of OCP and impedance modulus at 3 mHz ($|Z|_{3mHz}$) measured during the course of immersion are presented in Fig. 4. Bode and Nyquist diagrams for all repetitions are presented in Supplement material (Figs. S4–S6). Impedance at low frequencies represents total polarization resistance of the coating and it is proportional to the corrosion resistance of a coating.[81–83] For ZrCC samples the impedance modulus was $3 \cdot 10^5$ Ω·cm^2 after 1 h of immersion in 0.5 M NaCl; however, it increased over one order of magnitude during the first 6 to 7 days of immersion reaching the average value of $7.5 \cdot 10^6$ Ω·cm^2. After 10 days of immersion, $|Z|_{3mHz}$ impedance modulus formed a plateau at the average value $8.5 \cdot 10^6$ Ω·cm^2 (Fig. 4b). The same trend was noticed with Bode phase angles diagrams (Figs. S4–S6) where phase angle at low frequencies (ϕ, ∘) continuously increased up to 20 days of immersion, or even longer, depending on the sample. The highest increase was noted during the first 10 days of immersion indicating self-sealing /active corrosion protection within ZrCC. Drops in $|Z|_{3mHz}$ and ϕ occurred after 20 days of immersion (Fig. 4b) but afterwards $|Z|_{3mHz}$ recovered to a higher average value of $6.5 \cdot 10^6$ Ω·cm^2; this indicates increased probability that pitting will occur after 20 days of immersion in 0.5 M NaCl solution. Finally, after 30 days of immersion, a decrease in $|Z|_{3mHz}$ and ϕ indicates that samples underwent pitting corrosion.

According to Buchheit et al., if conversion coating applied on AA3003 exhibits R_c (defined as apparent integrated pitting resistance) of $2.3 \cdot 10^7$ Ω·cm^2 (range $1.1 \cdot 10^7$ to $4.8 \cdot 10^7$ Ω·cm^2) after 168 h immersion in 0.5 M NaCl, it has a probability of >80% to pass 168 h neutral salt spray test (NSST) test.[84,85] It was pointed out that EIS is more sensitive than salt spray chamber exposure for detecting the corrosion of a coating when the inspection interval was > 24 h.[85] The ZrCCs on AA3005 showed exceptional performance with impedance modulus of $8.5 \cdot 10^6$ Ω·cm^2 after 168 h of immersion. This value is smaller than that proposed by Buchheit et al.[85] but it has to be taken into account that the low frequency limit was higher than in the present work (10 mHz and 3 mHz, respectively). When taking that into account, the fitted average values of EIS parameters obtained in this work are R_c (96 h) = $1.2 \cdot 10^7$ Ω·cm^2 and R_c (168 h)=$1.61 \cdot 10^7$ Ω·cm^2 after 96 h and 168 h of immersion in 0.5 M NaCl. Based on these values we therefore assume that the coatings will pass 168 h NSST mark.[84,85] More data are given in supplement material (Table SVII.)

The time dependence of EIS spectra and progressive improvement of corrosion resistance is in agreement with results of PD measurements indicating that ZrCC coating on AA3005 has excellent corrosion performance, even better than TCP conversion coatings.[71,72] During the course of immersion in NaCl, the time dependence of OCP indicate that ZrCCs act as anodic inhibitors: OCP shifted from approximately −0.9 V after 1 h of immersion, to −0.7 V after 24 h of immersion, reaching values −0.6 V to −0.65 V after 10 days of immersion (Fig. 4a). Trends in OCP and impedance modulus were in correlation since the drop in $|Z|_{3mHz}$ was followed by a drop in OCP, as characteristic for pitting and exposure of AA3005 substrate to the electrolyte.

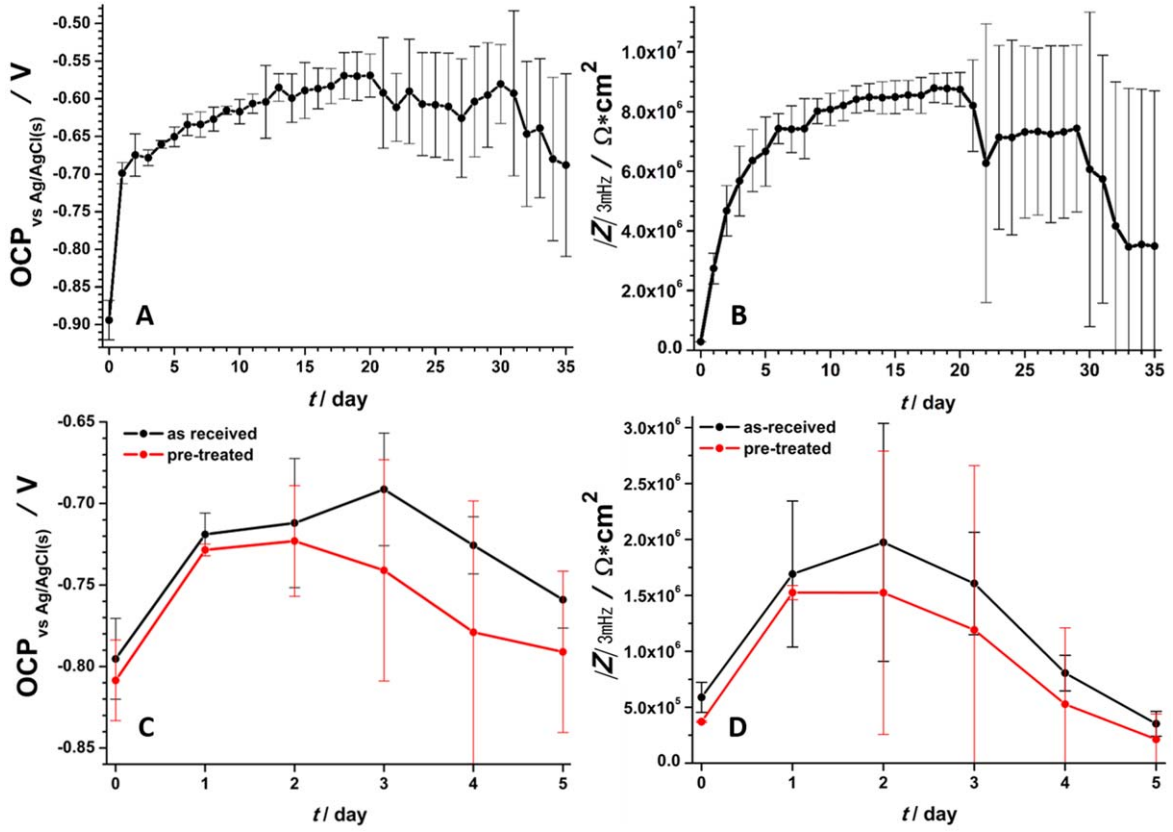

Figure 4. Impedance module at 3 mHz and open circuit potential as a function of immersion time for: (a, b) zirconium conversion coated AA3005; (c, d) as-received AA3005 (black symbols) and chemically pre-treated AA3005 (red symbols). Average values of 3 repetitions on different samples are presented by solid curves and standard deviation as error bars. Lines were drawn to guide the eye.

Compared to ZrCCs coated samples, the EIS behavior was quite different for bare and chemically pre-treated samples. For the latter, the $|Z|_{3mHz}$ showed an initial increase with immersion time but the values are approximately 3–4 times smaller compared to ZrCCs coated samples (Fig. 4d) and reached the maximum of $2.0 \cdot 10^6\ \Omega \cdot cm^2$. However, this value is still comparatively high and indicates that even bare AA3005 has substantial corrosion resistance. At longer immersion times, $|Z|_{3mHz}$ decreased, reflecting the initiation of the localized corrosion process. The time dependencies of OCP and Bode plots show a similar trend (Fig. 4c, S5). The same trend was noted with Bode phase angle plots (Fig. S5). Chemically pre-treated AA3005 showed very similar behavior as bare AA3005 but it was less corrosion resistant which is in good agreement with PD curves (Fig. 3, Table I).

SEM/EDS characterization of the coating surface.—SEM images of surface morphology and microstructure of chemically pre-treated AA3005, as-prepared ZrCC coated AA3005, and after immersion in NaCl are given in Fig. 5 recorded at lower and higher magnification. As-prepared ZrCC (Fig. 5b) was obviously very thin as no significant change was observed at the majority of the surface using SE at lower magnification mode compared to a chemically pre-treated sample (Fig. 5a, 5b). At higher magnification the coating is visible, especially around IMPs (inset in Fig. 5b). After 2 days of immersion in 0.5 M NaCl, the most significant feature was the appearance of a bloated area around IMPs (denoted as a "hat") (Fig. 5c). After 5 days of immersion, this area was not bloated anymore. There were no visible corrosion or pits in conversion coatings after 5 days of immersion in 0.5 M NaCl.

As-received AA3005 was composed of: Al (96.7 at. %), O (1.8 at. %), Mn (0.6 at. %), Fe (0.3 at. %), Mg (0.5 at.%) and Si (0.1 at. %) (Table II). The microstructural characteristics of AA3005 were typical as reported for this alloy.[86,87] The main intermetallic particles were Al_6(Mn, Fe) composed of Mn and Fe in an atomic ratio approximately 1, 1.3 and 1.6, respectively, for each spot, (Fig. 6a, spot 3, Table II and Fig. 6b, spots 4, 5, Table III). α-Al(Fe, Mn)Si IMPs containing Mn, Fe and Si were also detected (Fig. 6a, spot 4, Table II and Fig. 6b, spots 3, 6, Table III). The atomic ratios Mn/Fe and Mn/Si were similar, i.e. between approximately 1 and 2 (Table III). A large number of dispersoids (little white dots) sized below 1 μm containing mainly of Mn were present (Fig. 6a spot 2, Table II). There were no visible changes in the microstructure and elemental composition of AA3005 after alkaline cleaning using Metaclean (Fig. 6b, Table III). This confirms that Metaclean pre-treatment removed just grease and organic contamination from the surface.

SEM-BSE images of the as-prepared ZrCC and after immersion in 0.5 M NaCl for 2 and 5 days are presented in Figs. 7b–7d (SE images are presented in Fig. 5b–5d). For the sake of comparison, Fig. 6b for chemically pre-treated AA3005 is repeated as Fig. 7a. These samples were analysed by point EDS using an electron beam voltage of 3 kV or 11 kV corresponding to the analysed depth of approximately 100 nm and 1 μm, respectively (Tables IV–VII and SII–SIV). Results of EDS point analysis are presented in the form of atomic ratios (Table IV) or atomic % (Tables V–VII and SII–SIV). Further, EDS mapping was recorded for all the samples at 3 kV electron beam voltage (Fig. 8).

After conversion for 10 min in the conversion bath, the formation of ZrCC was completed over the whole surface (Fig. 7b and Tables IV, VII, SIII). The coating was cracked and much thicker at the (Mn, Fe) IMPs and in their proximity. These areas are denoted as hats. The atomic ratios of O/Zr, F/Zr and Al/Zr in the matrix of the as-prepared ZrCC were 2.39, 0.61 and 4.86 respectively (Fig. 7b, spot 2, Table VII), while the atomic ratios of O/Zr and F/Zr in coating at the hat above (Mn, Fe) IMPs were 1.68 and 0.31, respectively (Fig. 7b, spot 4, Table VII). The latter values indicate that the hat consists of $ZrO_{1.68}F_{0.31}$ and does not contain Al. There were darker areas in the coating with a smaller concentration of Zr, F and O, and a higher concentration of Al indicating that coating was thinner at these areas (Fig. 7b, spot 5, Table IV). EDS mapping

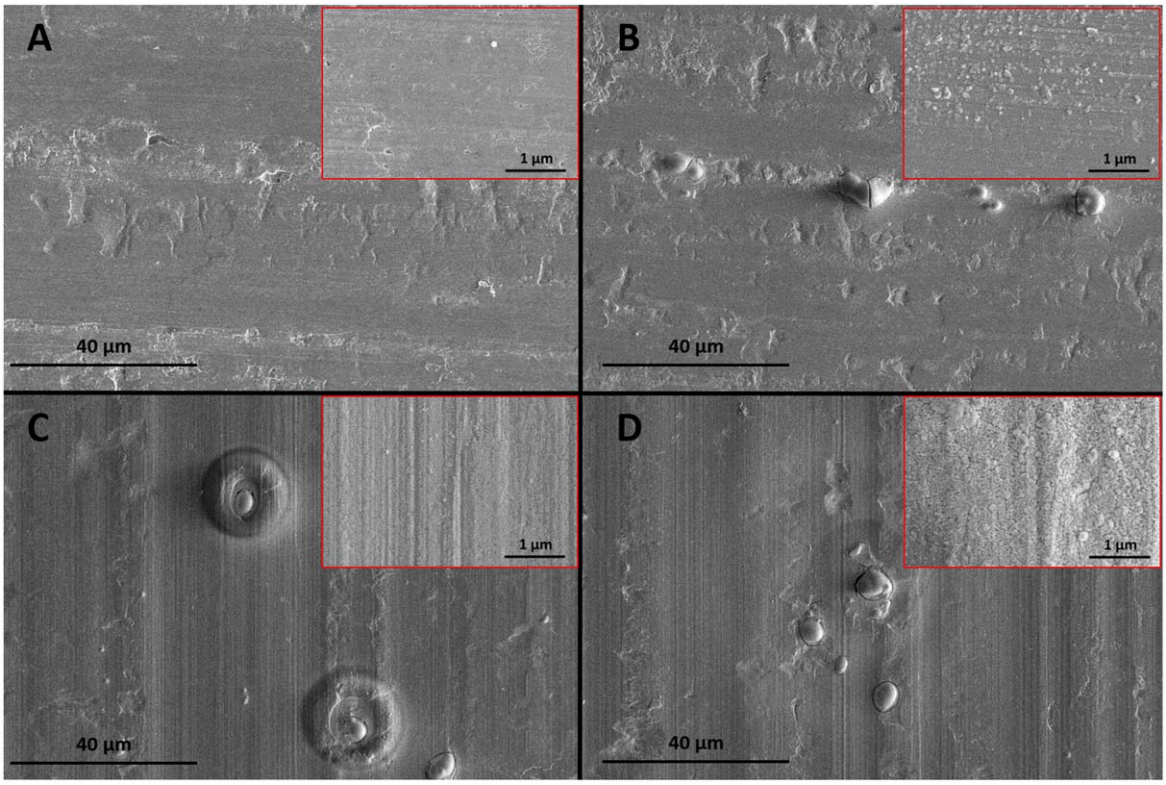

Figure 5. SEM secondary electron images of AA3005: (a) pre-treated with Metaclean; (b) zirconium conversion coating as prepared; (c) zirconium conversion coating after 2 days of immersion in 0.5 M NaCl and (d) zirconium conversion coating after 5 days of immersion in 0.5 M NaCl. Insets show images at higher magnification.

Table II. EDS analysis of as-received (bare) AA3005 (Fig. 6a); electron beam voltage of analysed spots 1–3 was 3 kV (denoted 1-4) or 11 kV (denoted 1*-4*) differing in the depth on the analysed region (approximately 100 nm and 1 μm, respectively).

Spot	at.% Al	at.% O	at.% Mn	at.% Fe	at.% Mg	at.% Si
1	89.2	10.4	—	—	0.4	—
2	87.5	12.1	—	—	0.4	—
3	79.2	20.8	—	—	—	—
4	81.5	18.5				
1*	96.7	1.8	0.6	0.3	0.5	0.1
2*	98	1.5	—	—	0.5	—
3*	79.3	2.8	8.8	9.0	—	—
4*	83.6	4.1	5.0	3.2	—	4.1

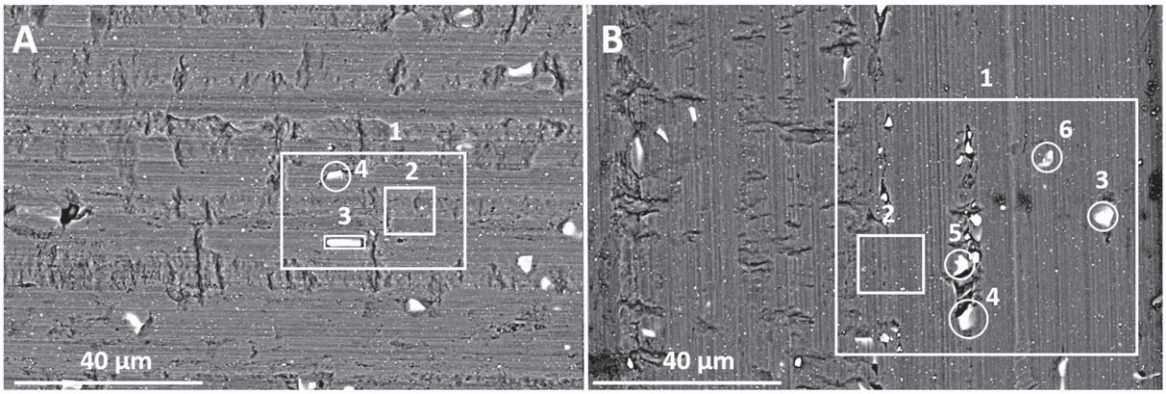

Figure 6. SEM-BSE images of (a) as-received and (b) chemically pre-treated AA3005. Squares 1, 2 and 3 denote spots where EDS analysis was carried out (Table II).

clearly shows that ZrCC was preferentially formed at and around IMPs (Fig. 8).

After 2 days of immersion in a 0.5 M NaCl solution, the most visible change at the coating was a dark circle around (Mn, Fe) IMPs (Fig. 7c and Tables V, VII, SIII). Apparently the cracks around (Mn, Fe) IMPs were weak spots in the coating where electrolyte penetrated and the corrosion process initiated. This would usually lead to the dissolution of IMPs, degradation of conversion coating and pit growth but in this case a densification and closing of cracks/pit around (Mn, Fe) IMPs occurred. This is clearly visible from EDS analysis/mapping which shows a very high concentration of O (65.8 at.%) and Al (30.7 at.%) at dark circle area around (Mn, Fe) IMPs indicating the formation of mostly oxide-containing area (Fig. 7c, spot 5, Table V). The atomic ratio of O/Zr at the hat increased to 2.69, while Al and F were not detected (Fig. 7c, spot 4, Table VII); therefore, the composition changed from $ZrO_{1.68}F_{0.31}$ to $ZrO_2 \cdot 0.7\ H_2O$. This indicates that the process of densification and closing of pores occurs in the whole coating and not just around (Mn, Fe) IMPs. The most significant change in ZrCC occurred during immersion in NaCl was a 5-fold reduced concentration of fluorine, i.e. from 6.9 at.% down to 1.3 at.% (Tables IV, V, spot 2). Atomic ratios of Al/Zr, O/Zr and F/Zr changed to 5.63, 2.86, and 0.125 (Fig. 7c, spot 2, Table VII). A decrease in fluorine concentration in the ZrO_2 hats and around them is clearly visible from EDS mapping (Fig. 8).

After 5 days of immersion in 0.5 M NaCl solution most visible change was a change of the dark circle around the Zr-oxide hat from dark to light white color with further spreading to a surrounding area (Fig. 7d and Tables VI, VII, SIV). It was difficult to select the right area for the comparison due to different samples. The area selected to be similar as in Fig. 7c seems to contain a significantly reduced O concentration (down to 31.0 at.%) and increased concentrations of Zr and Al (up to 10.2 at% and 57.7 at.%, respectively) (Fig. 7d, spot

Table III. EDS analysis of chemically pre-treated AA3005 (Fig. 6b); electron beam voltage of analysed spots 1–3 was 3 kV (denoted 1-6) or 11 kV (denoted 1*-6*) differing in the depth on the analysed region (approximately 100 nm and 1 μm, respectively).

Spot	at.% Al	at.% O	at.% Mn	at.% Fe	at.% Mg	at.% Si
1	88.8	10.6	—	—	0.6	—
2	88.8	10.6	—	—	0.6	—
3	82.3	17.7	—	—	—	—
4	83.1	16.9	—	—	—	—
5	82.4	17.6	—	—	—	—
6	87.7	12.3	—	—	—	—
1*	96.6	1.9	0.6	0.3	0.5	0.1
2*	97	1.8	0.5	0.1	0.5	—
3*	78.4	2.1	7.2	7.8	0.2	4.3
4*	87.3	3.7	5.0	3.9	—	—
5*	88.2	3.7	4.7	3.0	0.4	—
6*	87.9	2.0	5.1	2.5	—	2.6

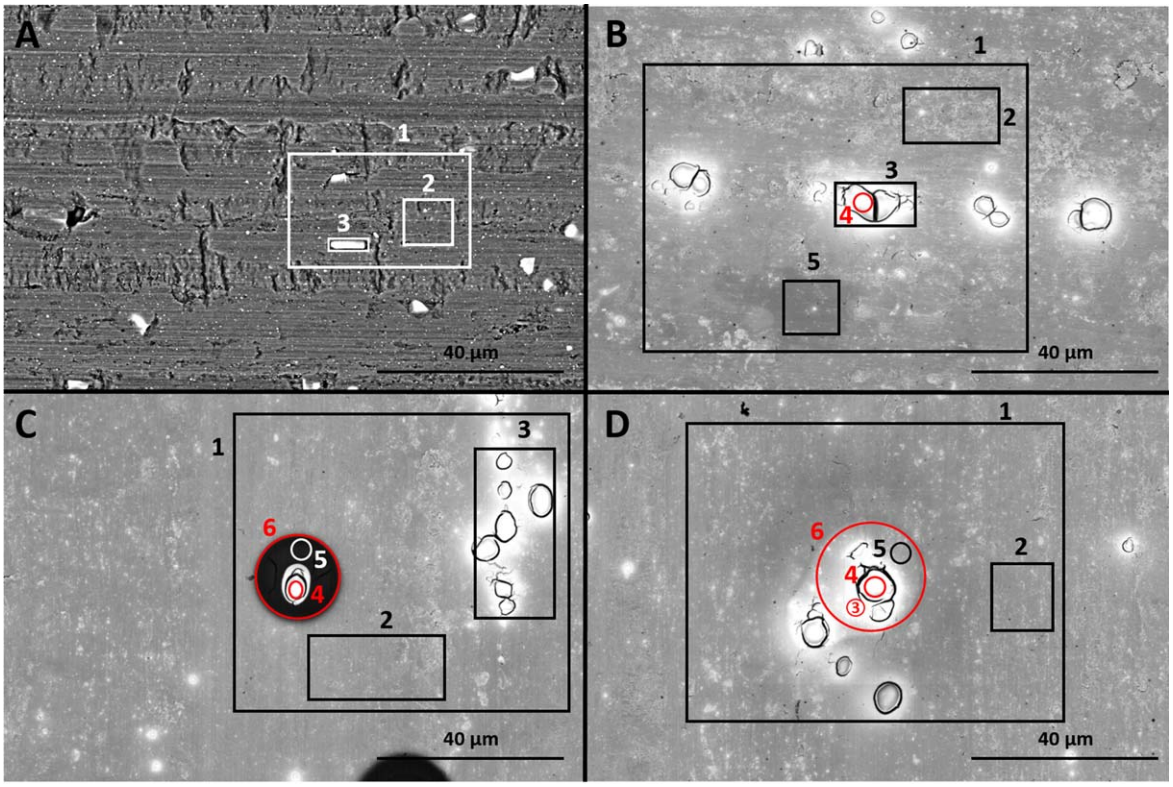

Figure 7. SEM-BSE images of AA3005: (a) pre-treated with Metaclean; (b) zirconium conversion coating as prepared; (c) zirconium conversion coating after 2 days of immersion in 0.5 M NaCl and (d) zirconium conversion coating after 5 days of immersion in 0.5 M NaCl. EDS mapping of areas denoted by square 1 is presented in Fig. 8. Squares 1, 2, 3, 4, 5, 6, present spots in Tables IV–VI and SII–SIV. Figure 7a is the same as 6b and is given for comparison's sake.

Table IV. EDS analysis of as-prepared zirconium conversion coatings on AA3005 (Fig. 7b); electron beam voltage of analysed spots 1–5 was 3 kV corresponding to the depth on the analysed region of approximately 100 nm. The results of the analysis carried out at 11 kV are presented in Table SII.

Spot	at.% Al	at.% Zr	at.% O	at.% F
1	55.4	12.7	25.5	6.4
2	54.9	11.3	27.0	6.9
3	22.3	23.9	45.1	8.7
4	—	33.5	56.2	10.3
5	74.9	7.6	13.9	3.6

5, Table VI) compared to that after 2 days immersion. The fluorine concentration was only 1.3 at.%. Atomic ratios Al/Zr, O/Zr and F/Zr were 5.14, 3.15 and 0.142 (Fig. 7d, spot 2, Table VII) indicating further densification of ZrCC. In the zirconium oxide hat the atomic ratio O/Zr was 3.16 (Fig. 7d, spot 4, Table VII).

Table V. EDS analysis of zirconium conversion coatings on AA3005 immersed in 0.5 M NaCl solution for 2 days (Fig. 7c); electron beam voltage of analysed spots 1–6 was 3 kV corresponding to the depth on the analysed region of approximately 100 nm. The results of the analysis carried out at 11 kV are presented in Table SIII.

Spot	at.% Al	at.% Zr	at.% O	at.% F
1	53.1	10.9	34.6	1.4
2	58.6	10.4	29.7	1.3
3	33.0	17.8	47.8	1.5
4	—	27.1	72.9	—
5	30.7	0.7	65.8	2.8
6	30.3	5.0	62.1	2.6

Summarizing, during the course of immersion in NaCl, the Al/Zr and O/Zr ratios at the coating matrix increased and that of F/Zr decreased indicating densification with Al- and Zr-oxides and depletion with fluoride or oxyfluoride. At the hat above (Mn,Fe) IMPs, Al was not detected and F was detected only prior to immersion. A change of O/Zr ratio reflects a progressive transformation from $ZrO_{1.68}F_{0.31}$ to $ZrO_2 \cdot 0.7\ H_2O$ and finally $ZrO_2 \cdot 1.2\ H_2O$.

SEM/EDS characterization at the coating cross-section.—SEM images of cross section and related EDS mapping of as-prepared ZrCC and ZrCC after 5 days immersion in 0.5 M NaCl were taken in the region near (Mn, Fe) IMPs of the AA3005 sample (Fig. 9). In this area the coating was thicker and its structure is fully developed. The thickness of the coating before and after immersion in NaCl solution was 200 nm. Based on SEM images and EDS mapping it appears that coating had a tri-layer structure. In the as-prepared ZrCC, Zr and O were concentrated in the upper layer of the coating, while F, Mn, Mg were equally distributed across whole coating (Fig. 9a). Distribution of elements in ZrCC changed after 5 days of immersion in 0.5 M NaCl: an upper layer of the coating consisted mainly of Zr, Mg and Mn; the middle layer consisted of O, F and Al, while the bottom layer contained mainly Al, O, F, Mn and Mg (Fig. 9b).

Atomic ratios of elements within ZrCC better describe the structure of coatings (Table VIII). (Please note that the atomic concentrations at spots 1–4 were reconstructed from EDS maps where the analysis spot is larger than the analyzed spot. Therefore, relative error is always similar and allows for relative comparison of concentrations). Atomic ratios O/Zr, Al/Zr, Mg/Zr increased from the upper to the inner part of the ZrCC coating indicating the enrichment of the inner part with Al, O, F and Mn. Ratios F/Zr and Mn/Zr were lower, or F and Mn were not detected at all, in the middle layer of ZrCC. In the bottom layer of the ZrCC, atomic ratios F/Zr and Mn/Zr were higher in comparison with the top layer of coating.

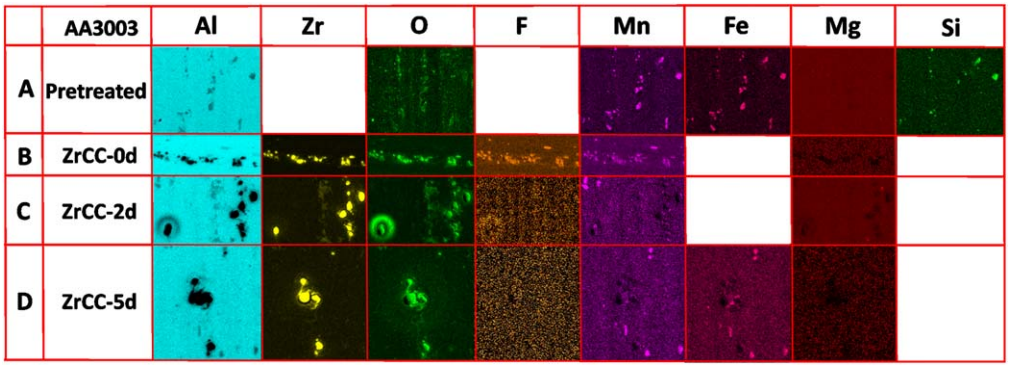

Figure 8. EDS mapping of AA3005 at the area marked in Fig. 7: (a) pre-treated with Metaclean; (b) zirconium conversion coating as-prepared (ZrCC-0d); (c) zirconium conversion coating after 2 days of immersion in 0.5 M NaCl (ZrCC-2d) and (d) zirconium conversion coating after 5 days of immersion in 0.5 M NaCl (ZrCC-5d).

Table VI. EDS analysis of zirconium conversion coatings on AA3005 immersed in 0.5 M NaCl solution for 5 days (Fig. 7d); electron beam voltage of analysed spots 1–6 was 3 kV corresponding to the depth on the analysed region of approximately 100 nm. The results of the analysis carried out at 11 kV are presented in Table SIV.

Spot	at.% Al	at.% Zr	at.% O	at.% F
1	53.9	11.0	33.7	1.4
2	54.5	10.6	33.4	1.5
3	9.4	23.5	67.2	—
4	—	24.0	76.0	—
5	57.7	10.2	31.0	1.1
6	35.2	18.7	45.0	1.1

The same trend was found after 5 days of immersion in 0.5 M NaCl (Table VIII). A substantial increase in O/Zr ratio up to 17.75 was noticed at the coating/substrate interface, and increased Mn/Zr and Fe/Zr ratios are the most significant changes. These indicate that Mn, Fe and O were incorporated in the bottom layer. The ratio of F/Zr was larger as well compared to the coating top. These findings are in agreement with SEM/EDX analysis of coating (Figs. 5–8) and confirm the densification and self-sealing of ZrCC during immersion in a 0.5 M NaCl solution.

SEM images and EDS mapping of the cross-sections of as prepared ZrCC and a Zr-oxide hat above an (Mn, Fe) intermetallic particle are presented in Fig. 10. As shown by EDS mapping, the hat was composed mainly of Zr, O, F and Al with atomic ratios for O/Zr, F/Zr Al/Zr of 1.31, 0.23 and 0.34, respectively (Figs. 10c, 10e and Table IX, spot 1). IMPs had an Mn/Fe atomic ratio of 0.65 (Fig. 10b, spot 2, S5). Fig. 10d presents the cross-section taken in the proximity of an IMP (detailed in Fig. 10b and imaged at higher magnification in Fig. 9a). The coating was uniform in the proximity of (Mn, Fe) IMPs. It had a tri-layer structure with a thickness of 200 nm.

Table VII. Atomic ratios in the matrix area of zirconium conversion coatings and at the hat for as-prepared ZrCC and ZrCC immersed in 0.5 M NaCl solution for 2 and 5 days. Atomic ratios were calculated from spots 2 and spots 4 (Figs. 7b–7d and Tables IV–VI) for matrix area and hat respectively.

Sample	Al/Zr	O/Zr	F/Zr
ZrCC-0d, spot 2	4.86	2.39	0.61
ZrCC-2d, spot 2	5.63	2.86	0.125
ZrCC-5d, spot 2	5.14	3.15	0.142
ZrCC- *hat*−0d, spot 4	—	1.68	0.31
ZrCC- *hat*−2d, spot 4	—	2.69	—
ZrCC-*hat*−5d, spot 4	—	3.16	—

SEM images and EDS mapping of the cross-sections of ZrCC and Zr-oxide hat above (Mn, Fe) IMP after 5 days of immersion in 0.5 M NaCl are presented in Fig. 11. As shown by EDS mapping, the hat was composed mainly of Zr, O and Al with atomic ratios for O/Zr, Al/Zr of 1.41 and 0.25, respectively (Figs. 11c, 11e and Table X, spot 1). The main change in the composition of Zr-oxide hat was the complete disappearance of F. IMPs had an Mn/Fe atomic ratio of 0.75 (Fig. 11c, spot 2) and 1.42 (Fig. 11c, spot 3). In the area between two IMPs there was a dense layer of Al, O and Zr with atomic ratios Al/Zr, O/Zr of 5.33 and 5.63, respectively (Fig. 11c, spot 4). It seems that the corrosion process was initiated around (Mn, Fe) IMPs but the channels around them then filled with a dense layer of aluminum oxide and passivated after 5 days of immersion in a 0.5 M NaCl solution. A small amount of Mn, Fe, F and Zr was present in aluminum oxide as well. These elements may be therefore incorporated in the growing layer of aluminum oxide formed around and above (Mn, Fe) IMPs (Fig. 11e). Figure 11d presents the cross-section taken in the proximity of IMP (detailed in Fig. 11b and imaged at higher magnification in Fig. 9b). The coating was uniform and undamaged in the proximity of (Mn, Fe) IMPs even after 5 days of immersion in 0.5 M NaCl. It had a tri-layer structure with a thickness of 200 nm.

TEM characterization of the coating cross section.— Transmission electron images of cross-sectioned ZrCC taken at the coating matrix are presented in Fig. 12. As-prepared ZrCC exhibited a tri-layer structure with a total thickness of 29 nm. The top layer had a thickness of 21.5 nm, middle layer 5 nm and the inner layer 2.5 nm. The coating was homogenous and without cracks. It is noteworthy that there is a difference in thickness obtained using SEM (Figs. 9–11) and TEM (Fig. 12) analyses, the latter being much smaller. This difference can be ascribed to the uneven thickness of the coating over the AA3005 surface, i.e., the coating is much thicker at and around the IMPs (Figs. 7, 9, 10, 11) than at the matrix (Fig. 12). The ratio between thickness near (Mn, Fe) IMPs and coating matrix far from IMPs ($d_{ZrCC\text{-}IMPs}/d_{ZrCC}$) was 6.9 as determined based on SEM and TEM analyses, respectively.

Based on the thickness of individual layers within the coating determined by TEM analysis (Fig. 12), the contribution of individual layers before and after immersion in NaCl was calculated (Table XI). Based on such normalized layer thickness it can be stated that the contribution of the top layer decreased from 74.2% to 49.2%; the middle layer increased from 17.2 to 21.0%, and that of bottom layer increased from 8.6% to 29.8%. These findings are in good correlation with SEM/EDS data that confirmed an increased concentration of O, Mn and Fe in bottom layers of ZrCC after 5 days of immersion in NaCl (Fig. 9). ZrCC was still homogenous; no cracks or pores were observed and the coating seemed denser and more compact in comparison with as-prepared ZrCC (Figs. 12b, 12d).

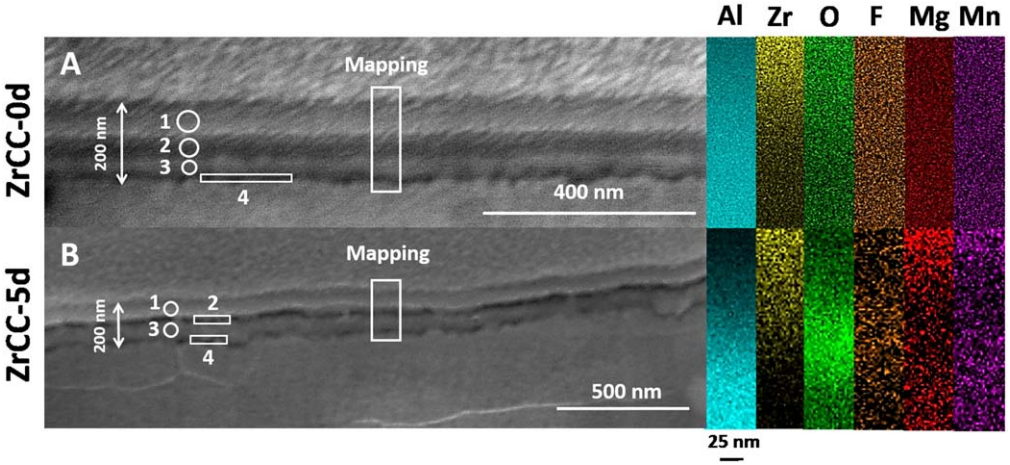

Figure 9. SEM images and EDS mapping of a cross-section of zirconium conversion coatings on AA3005: (a) zirconium conversion coating as-prepared; (b) zirconium conversion coating after 5 days of immersion in 0.5 M NaCl. The area where the mapping was recorded is denoted by vertical rectangles, circles and horizontal rectangles denote the spots where EDS analysis was carried out (Table VIII).

Table VIII. EDS analysis given in atomic ratios of elements at the cross-section of as-prepared zirconium conversion coating on AA3005 (Fig. 9a) and after 5 days immersion in 0.5 M NaCl (Fig. 9b).

Spot	Al/Zr	O/Zr	F/Zr	Mn/Zr	Mg/Zr	Fe/Zr
as-prepared						
1	7.37	1.53	0.233	0.023	0.035	—
2	15.60	1.49	0.189	—	0.076	—
3	34.92	2.15	—	—	0.192	—
4	39.17	2.43	0.435	0.087	0.217	—
Mapping average	14.30	1.87	0.226	0.038	0.076	—
After 5 days immersion						
1	6.91	1.88	0.174	0.070	0.070	0.023
2	6.74	1.84	0.202	—	0.061	—
3	15.16	3.04	0.255	0.020	0.020	0.020
4	226.5	17.75	0.5	1.25	1	1
Mapping average	18.12	3	0.220	0.123	0.098	0.073

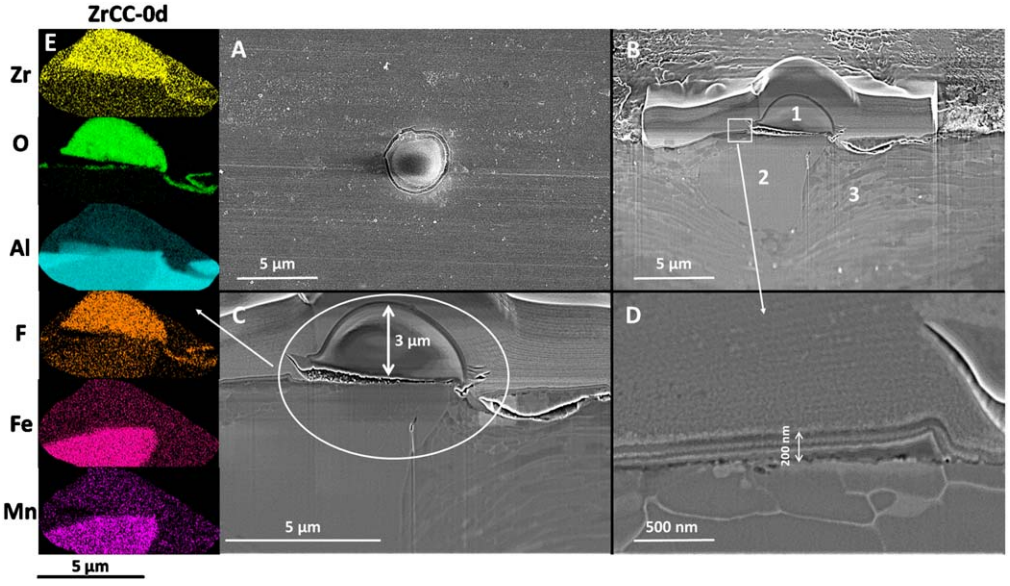

Figure 10. SEM images with EDS mapping of cross section of as prepared ZrCC. (a) top view, (b,c) side view, (d) the cross-section of coating in the proximity of (Mn, Fe) IMPs, as indicated by an arrow in (b), and (e) EDS mapping of the cross-section. The results of EDS analysis are given in Table IX and S5.

Table IX. EDS analysis of the cross-section of as prepared ZrCC at MnFe intermetallic particle (Fig. 10c). The results of the analysis carried out at 11 kV are presented in Table SV.

Spot	at.% Al	at.% Zr	at.% O	at.% F	at.% Mn	at.% Fe	at.% Mg
1	11.7	34.7	45.6	8.1	—	—	—
2	95.6	—	4.5	—	—	—	—
3	95.8	—	3.4	—	—	—	0.8

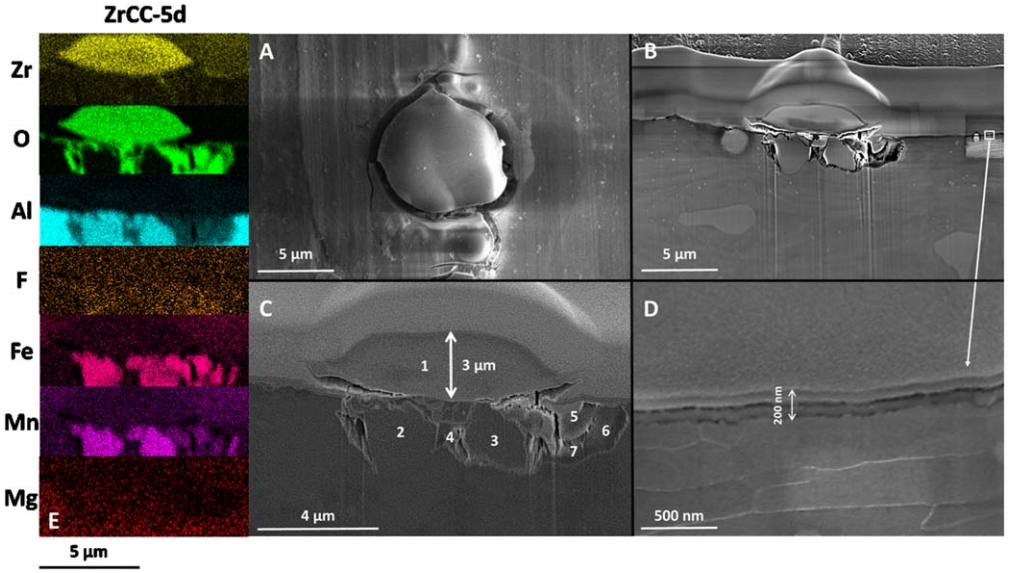

Figure 11. SEM images with EDS mapping of the cross-section of ZrCC after 5 days of immersion in a 0.5 M NaCl solution. (a) top view, (b,c) side view, (d) the cross-section of coating in the proximity of (Mn, Fe) IMPs, as indicated by an arrow in (b), and (e) EDS mapping of the cross=section. Results of EDS analysis are given in Table X, SVI.

XPS characterization of the coating surface.—XPS analysis was carried out on as-received and chemically pre-treated AA3005, as prepared ZrCC and ZrCC immersed in 0.5 M NaCl solution for 2 and 5 days. XPS technique has a probing depth up to 10 nm thus giving information from the upper-most layer of the ZrCC. The composition of samples deduced from XPS survey spectra are presented in Table XII. The surface of an as-received sample contained Al, O, Mg, and N, while chemically pre-treated sample contained Al, O, Mg, P, Si and Na. Na and P originate from Metaclean alkaline cleaner that contains $NaSiO_3$ and probably some P based corrosion inhibitor/surfactant. Chemical cleaning does not cause an enrichment in Mn (detected concentration < 0.2 at.%).

Aluminum and oxygen are related to the formation of aluminum oxide/hydroxide. After the conversion coating process with hexafluorozirconic acid, aluminum almost diminished due to coverage with ZrCC, as evidenced by the appearance of Zr and F originating from the conversion coating. After 2 days of immersion in NaCl, however, F completely disappeared from the top layer of ZrCC and, at the same time, Al appeared in the top layer. The concentration of Al increased with immersion time, while that of Zr decreased. Si appeared after 2 days of immersion in a 0.5 M NaCl solution and originates from AA3005.

High resolution XPS spectra recorded for major elements detected in survey XPS spectra are presented in Fig. 13. High resolution Al 2p spectra are presented in Fig. 13a. The Al 2p peak is usually presented as a single peak rather than two split component peaks $2p_{3/2}$ and $2p_{1/2}$. Two 2p peaks are noted in the Al 2p spectrum for as-received and chemically pre-treated Al centered at binding energy (E_b) 72.4 and 74.8 and corresponding to Al metal and $Al(OH)_3$, respectively.[88,89] Considering the intensity ratio between the two peaks, it can be stated that the surface is covered by a thin, few nanometers thick, the layer of $Al(OH)_3$ which allows the detection of Al metal. After the conversion coating process, however, peaks for Al diminished due to coverage of AA3005 with ZrCC. After 2 and 5 days of immersion, a small peak at 74.5 eV re-appeared suggesting the formation of $Al(OH)_3$ in the top layer of coating.

High resolution O 1 s spectra are presented in Fig. 13b. For as-received and chemically pre-treated samples, the peak was centered at 531.9 eV suggesting the prevalence of hydroxide over oxide.

Table X. EDS analysis of the cross-section of ZrCC at MnFe intermetallic particle after 5 days of immersion in 0.5 M NaCl solution (Fig. 11c). The results of the analysis carried out at 11 kV are presented in Table SVI.

Spot	at.% Al	at.% Zr	at.% O	at.% F	at.% Mn	at.% Fe	At.% Cu
1	9.4	37.3	52.5	0.8	—	—	—
2	74.6	—	4.1	—	9.1	12.2	—
3	76.4	—	3.4	—	12.2	8.6	—
4	44.2	8.3	46.7	0.8	—		—
5	27.1	0.9	53.8	0.4	—	17.8	—
6	50.9	—	40.1	0.9	1.4	3.1	3.5
7	41.8	0.5	48.9	4.0	-	4.7	-

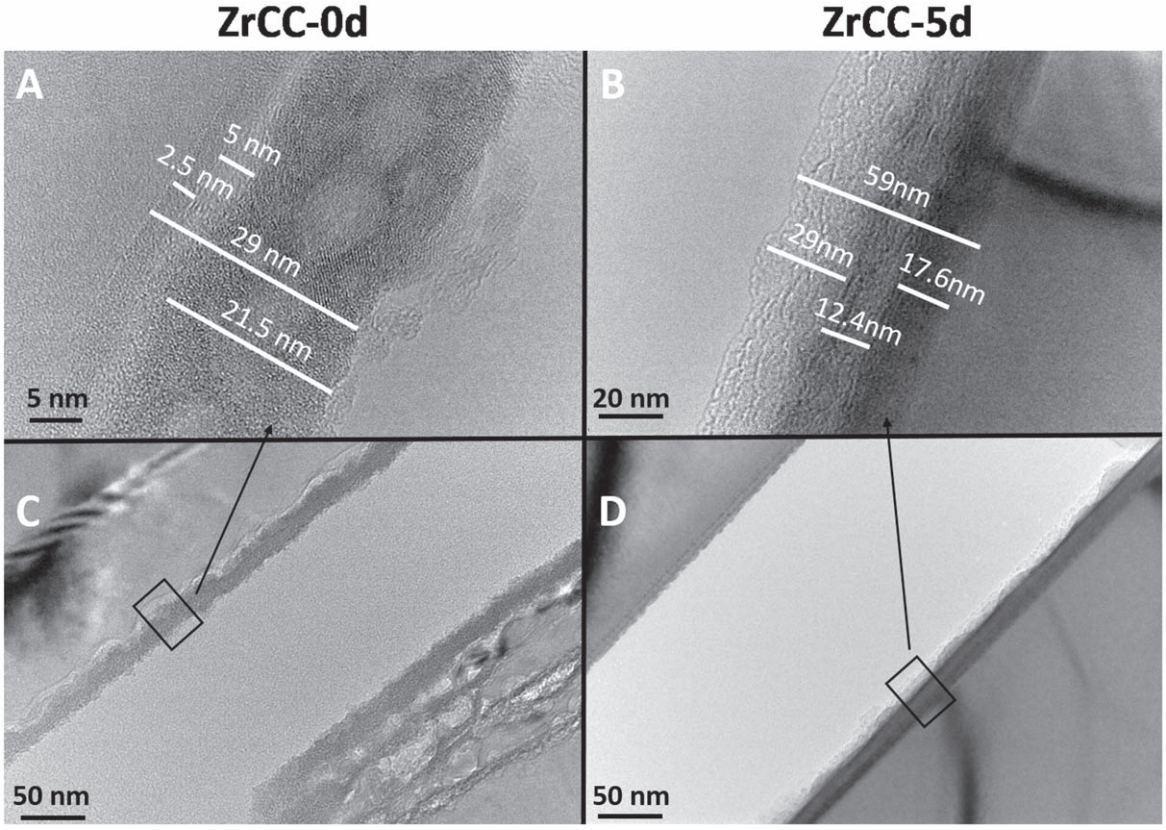

Figure 12. Transmission electron microscopy images of (a, c) as-prepared zirconium conversion coating and (b, d) after 5 days immersion in 0.5 M NaCl solution.

Table XI. Percentage of individual layer thickness to total coating thickness for as prepared zirconium conversion coating and zirconium conversion coating immersed in 0.5 M NaCl solution for 5 days (calculated from layer thickness in Fig. 12).

	ZrCC-0d	ZrCC-5d
Top layer, %	74.2	49.2
Middle layer, %	17.2	21.0
Bottom layer, %	8.6	29.8

Considering the presence of hydrated Zr oxide (see below), this peak could be deconvoluted into peaks for bound H_2O, $Al(OH)_3$ and $ZrO_2{\cdot}2H_2O$ at binding energies at 533 eV, 532 (531.9) eV and 531.5 eV, respectively.[89,90] After the conversion process, the O 1 s peak shifted to 531.2 eV and is now related to predominantly hydrated Zr oxide and/or oxyfluoride ($ZrO_2{\cdot}2H_2O$/ ZrF_xO_y). After 2 and 5 days of immersion ZrCC in a 0.5 M NaCl solution, the center of the O1 s peak was shifted back to slightly higher E_b of 531.6 eV corresponding to the presence of $ZrO_2{\cdot}2H_2O$ and $Al(OH)_3$.

The F 1s peak was located at E_b of 684.8 eV and was noted only for the as-prepared ZrCC indicating the presence of ZrF_4/ZrF_xO_y in the top layer of as-prepared coating (Fig. 13d). After 2 and 5 days of immersion, the F 1s peak disappeared, indicating dissolution of fluorine and transformation of ZrF_4/ZrF_xO_y into $ZrO_2{\cdot}2H_2O$.

High resolution spectra Zr 3d spectra recorded after the conversion coating process are presented in Fig. 13c. The Zr $3d_{5/2}$ and $3d_{3/2}$ peaks for the as-prepared coating are centered at 185.5 eV and 183.2 eV, respectively. Considering a relatively high fluorine and oxygen contents (Fig. S7), this spectrum reflects the presence of a mixture of ZrF_4/ZrF_xO_y and $ZrO_2{\cdot}2H_2O$.[91] After 2 and 5 days of immersion in 0.5 M NaCl solution, however, the peaks shifted to lower E_b of 184.9 eV and 182.5 eV, respectively, indicating the progressive transformation of Zr-fluoride/oxyfluoride to $ZrO_2{\cdot}2H_2O$. These findings are in correlation with the disappearance of the fluorine peak in the F 1s spectrum.

ToF-SIMS characterization of coating microstructure.—In order to analyse the coating structure and composition, ToF-SIMS negative ion profiles were recorded for as prepared ZrCC and for ZrCC immersed in 0.5 M NaCl solutions (Fig. 14). The sputtering

Table XII. Concentration of elements obtained by XPS analysis of as-received, chemically pre-treated and zirconium conversion coated AA3005 samples.

Sample	at.% Al	at.% Zr	at.% O	at.% F	at.% Mg	at.% Si	at.% P	at.% Na	at.% N	at.% Cl
as received	19.6	—	69.1	—	9.9	—	—	—	1.4	—
pre-treated	18.9	—	66.6	—	5.9	0.5	3.7	4.3	—	—
ZrCC-0d	1.0	23.4	67.2	8.4	—	—	—	—	—	—
ZrCC-2d	4.9	17.4	74.7	—	—	3.0	—	—	—	—
ZrCC-5d	8.1	14.6	69.2	—	—	—	—	—	—	8.1

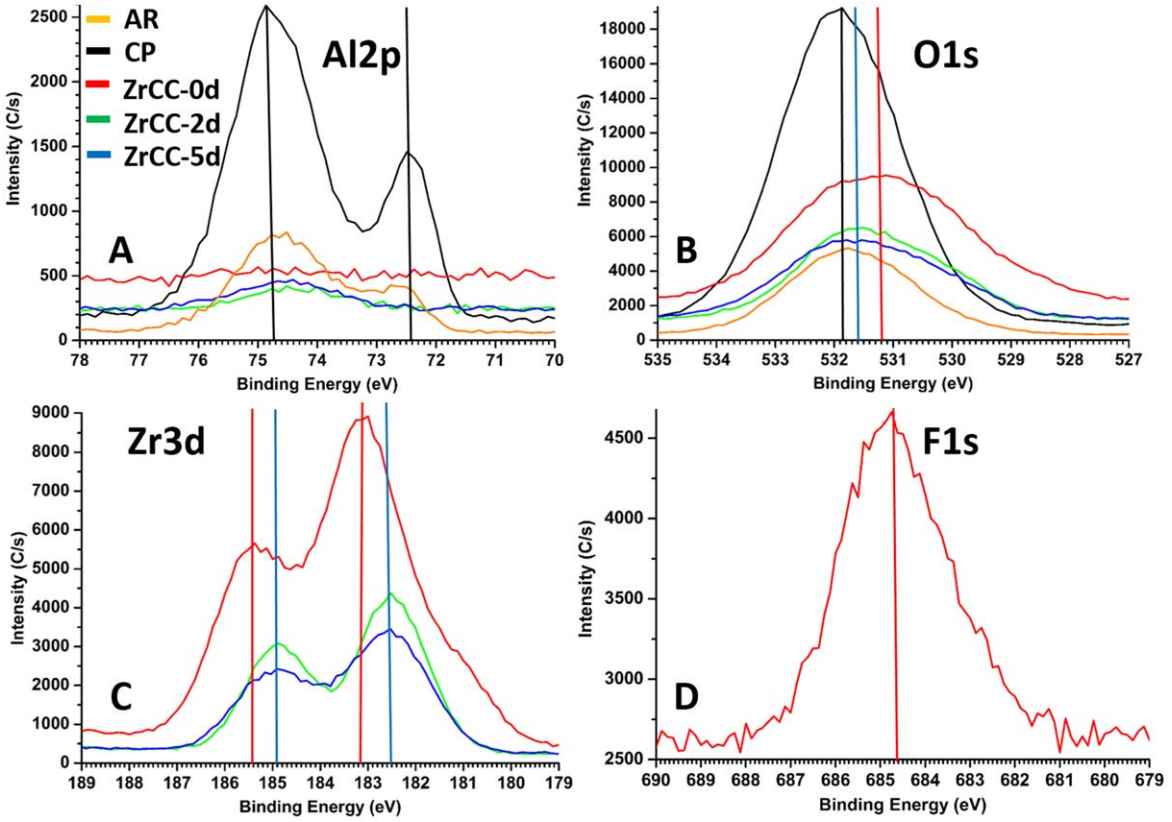

Figure 13. High resolution XPS spectra (a) Al 2p, (b) O 1 s, (c) Zr 3d in (d) F 1 s for as-received (AR) and chemically pre-treated (CP) AA3005 and zirconium conversion coatings on AA3005 as-prepared ZrCC and immersed in 0.5 M NaCl solution for 2 and 5 days. Spectra were not normalized on the intensity scale.

rate was 0.30 nm s^{-1} (± 0.02 nm s^{-1}). As-prepared ZrCC was approximately 30 to 40 nm thick. It consisted of an outer layer that had the highest concentration of ZrO^- and a lower concentration of $AlOF^-$ (Fig. 14, region 1); therefore, its structure can be correlated with $ZrO_2 \cdot 2H_2O/ZrO_xF_y$ species. A significant amount of CuO^- ions was detected in the outer layer. The highest amount of $AlOF^-$ ions was detected in the middle layer, accompanied with peaks for AlO-, MgO- and $Al_2O_4^-$ ions (Fig. 14, region 2). ZrO^- ions were present in the middle layer but in a smaller amount than in the outer layer. The same ions were found in the middle layer and at the interface (Fig. 13, region 3) so it was hard to distinguish the border between these two regions.

After 5 days of immersion in 0.5 M NaCl, the profile of ZrO^- ions remained approximately the same with a maximum in the outer layer (Fig. 14, region 1). The most important change was a decrease in intensity (concentration) of F^- and $AlOF^-$ ions. At the same time, the concentration of Cl^- ions increased significantly following the same profile shape as that of F^- and $AlOF^-$ ions. This indicates that Cl^- ions were exchanged with F^- ions and incorporated within the ZrCC structure. The concentration of AlO^- was larger throughout the ZrCC showing two maxima in the outer and, especially, the middle part, respectively. This increased concentration extended over the interface with the substrate for approximately 10–15 nm. This finding indicates the segregation of Al_2O_3 in middle layer/ interface of ZrCC which may be responsible for the increased corrosion resistance of ZrCC coating, as proved experimentally (Figs. 3 and 4).

In the course of immersion in NaCl, the intensity profile related to CuO^- ions decreased due to dissolution or ZrCC heterogeneities; that of MgO^- ions increased and was shifted deeper to the substrate as well. The amount of $Al_2O_4^-$ ions in the middle layer/ interface increased 2-fold. We correlate these ions with a spinel structure in middle/interface layers but this is only our speculations because it can be also correlated with aluminium oxide as well and other oxides.

Mechanism of active corrosion protection/self-sealing.— Electrochemical results obtained for zirconium conversion coatings on AA3005 suggest that these coatings enable self-sealing and active corrosion protection when immersed in a 0.5 M NaCl solution. These following results substantiate this statement: (i) rapid decay and recovery of OCP during the first 2 h immersion, (ii) a 50-fold increase in impedance modulus at 3 mHz and the ability to sustain it at values in the megaohm·cm^2 range ($7.5 \cdot 10^6$ to $9.5 \cdot 10^6$ Ω·cm^2) and to resist pitting up to at least 21 days, and (iii) increased passive window (from 0.22 to 0.45 V) and decreased corrosion current density of two orders of magnitude (from $2.32 \cdot 10^{-7}$ A·cm^{-2} down to $3 \cdot 10^{-9}$ A·cm^{-2}) after 10 days of immersion.

The electrochemical study was complemented with microstructural and compositional studies. The microstructural investigation by XPS showed the disappearance of fluorine in the top layer of ZrCC after 2 days in 0.5 M NaCl and the transformation of ZrF_4/ZrF_xO_y into $Zr(OH)_2 \cdot 1.2H_2O$ and $Al(OH)_3$. SEM/EDS investigation confirmed that the concentration of F decreased and that of Al and O increased during immersion. FIB/EDS investigation showed that coating was 200 nm thick in the proximity of IMPs, homogenous with tri-layer structure, while (Mn, Fe) IMPs were covered with a dense hat of zirconium oxide. During immersion in NaCl, channels around (Mn, Fe) IMPs became progressively filled with a dense layer of aluminum oxide containing a small content of Zr and F. This process results in the passivation of the IMPs. At the same time, (Mn, Fe) IMPs were dissolving, leading to the incorporation of Mn and Fe in ZrCC. We believe that their incorporation has a role in the stabilization of aluminum oxide around IMPs and contributes to the passivation. Especially important seems to be Mn which was integrated in the bottom layer of ZrCC accompanied with the

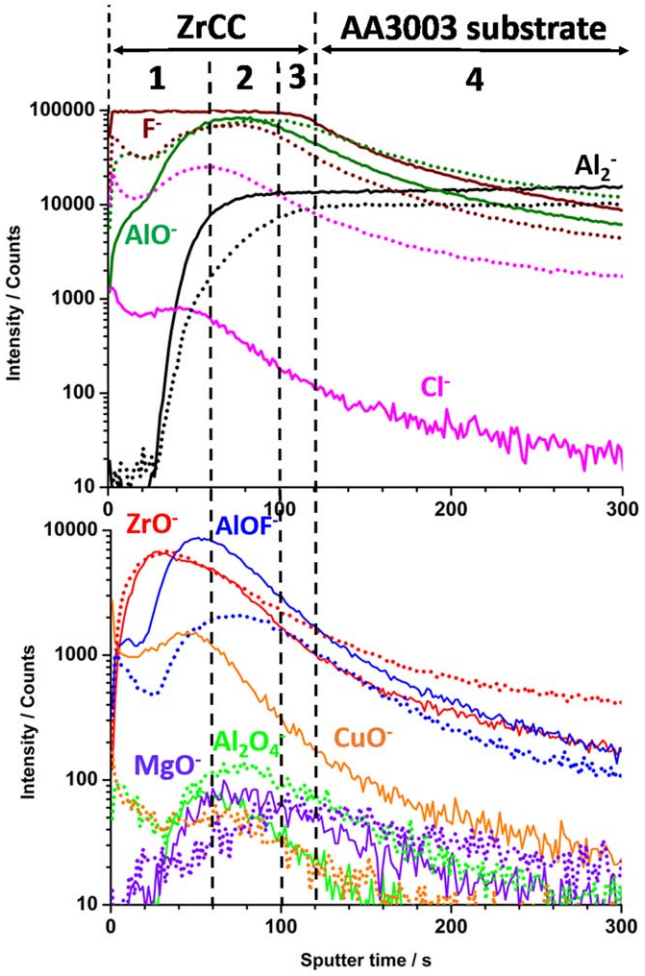

Figure 14. ToF-SIMS negative ions depth profiles of zirconium conversion coating applied on AA3005. (full lines)—as prepared ZrCC; (dotted lines)—ZrCC after 5 days of immersion in 0.5 M NaCl solution. 1-outer layer, 2-middle layer, 3-inner layer/or interface, 4-substrate.

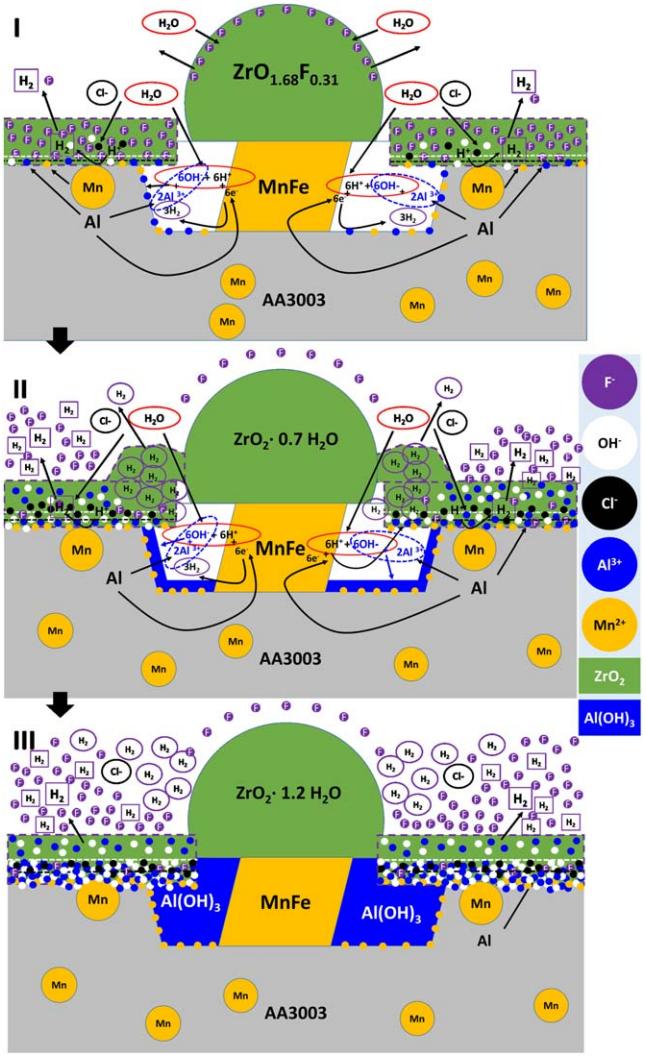

Figure 15. Self-sealing mechanism of zirconium conversion coating applied on AA3005 during its immersion in 0.5 M NaCl solution.

highest increase in O. TEM investigation showed that the tri-layer structure consisting of top, middle and bottom layer changed from 74.2%, 17.2%, 8.6% of layer in the as-prepared ZrCC to 49.2%, 21.0% and 29.8% after 5 days immersion in 0.5 M NaCl solution.

Based on these facts we propose the following mechanism of self-sealing/active corrosion protection in ZrCC applied on AA3005 (Fig. 15).

First, H_2O diffuses inside ZrCC through cracks and pores down to IMPs and Mn dispersoids where hydrogen evolution and oxygen reduction reactions take place. This leads to an increased concentration of OH^- and release of hydrogen gas (Eqs. 6 and 7). Released $H_{2(g)}$, especially around (Mn, Fe) IMPs, causes a bloating around IMPs after 2 days of immersion in NaCl (Fig. 7c). At the same time, OH^- ions cause a dissolution of aluminum oxide and its precipitation in the form of dense $Al(OH)_3$ around (Mn, Fe) IMPs thus closing cracks and channels (Eq. 8). Excess in OH^- ions together with $H_{2(g)}$ is transported towards outside part of ZrCC expelling F^- ions from the coating interior and thus transforming ZrF_4/ZrO_xF_y to $ZrO_2 \cdot 2\,H_2O_{(s)}$ (Eq. 9). Excess of F^- ions is transported to a solution where it is balanced with Na^+ ions. It can be also postulated based on obtained results that, along with the H_2 evolution reaction, manganese is dissolved from IMPs and dispersoids (Eq. 11). Dissolved Mn^{2+} incorporates in the bottom layer of ZrCC forming spinel $MnAl_2O_{4(s)}$ (Eq. 12). It is known that spinels have great chemical and thermal stability.[92,93]

$$H_2O \rightarrow 2H^+_{(aq)} + OH^-_{(aq)} \quad [6]$$

$$2H^+_{(aq)} + 2e^- \rightarrow H_{2(g)} \quad [7]$$

$$Al^{3+}_{(aq)} + 3OH^-_{(aq)} \rightarrow Al(OH)_{3(s)} \quad [8]$$

$$ZrF_4/ZrO_xF_{y(s)} + 4OH^-_{(aq)} \rightarrow ZrO_2 \times 2H_2O_{(s)} + 4F^-_{(aq)} \quad [9]$$

$$ZrF_4/ZrO_xF_{y(s)} + (4 + y)Cl^-_{(aq)} \rightarrow ZrCl_4/ZrO_xCl_{y(s)} + (4 + y)F^-_{(aq)} \quad [10]$$

$$Mn \rightarrow Mn^{2+}_{(aq)} + 2e^- \quad [11]$$

$$Al_2O_3 \cdot H_2O_{(s)} + Mn^{2+}_{(aq)} \rightarrow MnAl_2O_{4(s)} + 2H^+_{(aq)} \quad [12]$$

Conclusions

1. The formation of zirconium conversion coating on AA3005 was completed after 10 min of immersion in 200 ppm hexfluorozirconic acid bath at pH = 4.8 at room temperature.
2. Zirconium conversion coating applied to AA3005 showed excellent corrosion performance. Bode modulus at 3 mHz increased 50-fold during immersion in 0.5 M NaCl solution

and sustained at $7.5 \cdot 10^6$ Ω·cm^2 to $9.5 \cdot 10^6$ Ω·cm^2 for at least 21 days with no pitting observed. The shift of the open circuit potential in nobler direction indicates anodic inhibition behavior of these coatings.

3. The as-prepared coating was uniform with thickness that varied from 30 nm at the coating matrix up to 200 nm at/around IMPs. A tri-layer structure was noted, with the upper layer being enriched in Zr and O and bottom layer enriched in Al, F, Mn and Mg.
4. After immersion of 5 days in 0.5 M NaCl solution, the overall thickness of the coating did not change, but the proportion of individual layer changed, as well but the microstructure and composition. The thickness of the top layer decreased and that of the middle, and especially, the bottom layer increased. A transformation from ZrF_4/ZrO_xF_y to $ZrO_2 \cdot 1.2H_2O_{(s)}$ occurred suggesting densification and sealing of ZrCC. Mn segregated in the bottom layer of ZrCC.
5. Upon immersion in NaCl, a hat consisting mainly of ZrO_2 with a small amount of Al formed above and around (Mn, Fe) IMPs. However, at prolonged immersion channels around IMPs became filled with a dense layer of aluminum oxide leading to passivation. At the same time, the concentration of fluorine decreased, while that of O increased, especially in the middle and bottom layer of ZrCC.
6. Based on the above facts it can be stated that ZrCC on AA3005 alloy exhibits a self-sealing/active corrosion protection behavior during immersion in a 0.5 M NaCl solution. Its corrosion performance seems to be equal or better compared to that usually observed for chromium conversion coatings.[85]
7. It seems that Mn from AA3005 together with Zr from ZrCC are able to trigger a self-sealing and active corrosion protection within the coating by incorporation in the bottom part of the conversion coating. This is very promising results and we suggest that future formulas of ZrCC should include Mn.

Acknowledgments

This research was funded by Slovenian Research Agency, research core funding grant number PR-07023 and PR-0393. The authors thank Sandra Drev, PhD (Center for Electron Microscopy, Jožef Stefan Institute) for the preparation and imaging of samples with the transmission electron microscope. We acknowledge Centre of Excellence Nanocenter for the use of FEI Helios Nanolab 650 microscope. We also acknowledge Janez Kovač, PhD and Tatjana Filipič, MSc, for XPS and ToF-SIMS measurements (Department of Surface Engineering and Optoelectronics, Jožef Stefan Institute).

References

1. I. Milošev and G. S. Frankel, *J. Electrochem. Soc.*, **165**, C127 (2018).
2. D. B. Mitton, A. Carangelo, A. Acquesta, T. Monetta, M. Curioni, and F. Bellucci, *Corros. Rev.*, **35**, 365 (2017).
3. A. E. Hughes, in *Encyclopedia of Interfacial Chemistry*, ed. K. Wandelt (Elsevier, Oxford) p. 108 (2018).
4. M. Becker, *Corros. Rev.*, **37**, 321 (2019).
5. K. Ogle and R. G. Buchheit, "Conversion coatings." in *Encyclopedia of Electrochemistry* (Wiley) p. 460 (2007).
6. P. D. Deck, M. Moon, and R. J. Sujdak, *Prog. Org. Coat.*, **34**, 39 (1998).
7. W. Zhu, W. Li, S. Mu, Y. Yang, and X. Zuo, *Appl. Surf. Sci.*, **384**, 333 (2016).
8. F. Andreatta, A. Lanzutti, L. Paussa, and L. Fedrizzi, *Prog. Org. Coat.*, **77**, 2107 (2014).
9. M. A. Smit, J. A. Hunter, J. D. B. Sharman, G. M. Scamans, and J. M. Sykes, *Corros. Sci.*, **45**, 1903 (2003).
10. N. W. Khun, S. Adhikari, Y. Y. Li, G. S. Frankel, J. McGee, T. Smith, B. Bammel, and J. Zimmerman, *Corrosion*, **73**, 339 (2016).
11. J. H. Nordlien, J. C. Walmsley, H. Østerberg, and K. Nisancioglu, *Surf. Coat. Technol.*, **153**, 72 (2002).
12. H. Eivaz Mohammadloo and A. A. Sarabi, *Prog. Org. Coat.*, **101**, 391 (2016).
13. M. W. Kendig and R. G. Buchheit, *Corrosion*, **59**, 379 (2003).
14. O. Gharbi, S. Thomas, C. Smith, and N. Birbilis, *NPJ Materials Degradation*, **2**, 12 (2018).
15. T. S. N. Sankara Narayanan, *Reviews in Advanced Materials Science*, **9**, 130 (2005).
16. W. Rausch, *Finishing Publications Ltd. (UK)*, **1990**, 406 (1990).
17. Y. Guo and G. S. Frankel, *Surf. Coat. Technol.*, **206**, 3895 (2012).
18. H. Hubert, H. Puderbach, H. Pulm, and W. A. Roland, *Z. Anal. Chem.*, **333**, 304 (1989).
19. L. Fedrizzi, F. Deflorian, and P. L. Bonora, *Electrochim. Acta*, **42**, 969 (1997).
20. P. D. Deck and D. W. Reichgott, *Metal Fin.*, **90**, 29 (1992).
21. J. Qi, T. Hashimoto, J. Walton, X. Zhou, P. Skeldon, and G. E. Thompson, *J. Electrochem. Soc.*, **163**, C25 (2016).
22. T. R. Giles, B. H. Goodreau, W. E. Fristad, J. Kroemer, and M. Frank, *SAE Int. J. Mater. Manf.*, **1**, 575 (2008).
23. M. Doerre, L. Hibbitts, G. Patrick, and K. N. Akafuah, *Coatings*, **8**, 405 (2018).
24. T. R. Giles, D. R. Vonk, and S.-L. Favero, *Encontro e Exposição Brasileira de tratamento de superficie III INTERFINISH Latino Americano*, p. 172 (2012).
25. Y. Ota and T. Kojima, *Kobelco Technology Review*, **35**, 61 (2017).
26. R. Moore and B. Dunham, *Met. Finish.*, **106**, 46 (2008).
27. B. Dunham, *Met. Finish.*, **110**, 18 (2012).
28. Y. Guo and G. S. Frankel, *Corrosion*, **68**, 045002 (2012).
29. L. Li, G. P. Swain, A. Howell, D. Woodbury, and G. M. Swain, *J. Electrochem. Soc.*, **158**, C274 (2011).
30. M. Zhang, Z. Chen, Q. Chen, H. Zou, J. Lou, and J. He, *Mutation Research/Genetic Toxicology and Environmental Mutagenesis*, **654**, 45 (2008).
31. K. Ambreen, F. H. Khan, S. Bhadauria, and S. Kumar, *Toxicology and Industrial Health*, **30**, 405 (2014).
32. F. Andreatta, A. Turco, I. De Graeve, H. Terryn, J. H. W. De Wit, and L. Fedrizzi, *Surf. Coat. Technol.*, **201**, 7668 (2007).
33. O. Lunder, C. Simensen, Y. Yu, and K. Nisancioglu, *Surf. Coat. Technol.*, **184**, 278 (2004).
34. S. S. Golru, M. M. Attar, and B. Ramezanzadeh, *J. Ind. Eng. Chem.*, **24**, 233 (2015).
35. P. Santa Coloma, U. Izagirre, Y. Belaustegi, J. B. Jorcin, F. J. Cano, and N. Lapeña, *Appl. Surf. Sci.*, **345**, 24 (2015).
36. F. O. George, P. Skeldon, and G. E. Thompson, *Corros. Sci.*, **65**, 231 (2012).
37. G. Yoganandan, K. Pradeep Premkumar, and J. N. Balaraju, *Surf. Coat. Technol.*, **270**, 249 (2015).
38. X. Zhong, X. Wu, Y. Jia, and Y. Liu, *Appl. Surf. Sci.*, **280**, 489 (2013).
39. A. Sarfraz, R. Posner, M. M. Lange, K. Lill, and A. Erbe, *J. Electrochem. Soc.*, **161**, C509 (2014).
40. J. Cerezo, I. Vandendael, R. Posner, K. Lill, J. H. W. De Wit, J. M. C. Mol, and H. Terryn, *Surf. Coat. Technol.*, **236**, 284 (2013).
41. J. Cerezo, P. Taheri, I. Vandendael, R. Posner, K. Lill, J. H. W. de Wit, J. M. C. Mol, and H. Terryn, *Surf. Coat. Technol.*, **254**, 277 (2014).
42. J. Cerezo, R. Posner, I. Vandendael, J. H. W. de Wit, H. Terryn, and J. M. C. Mol, *Mater. Corros.*, **67**, 361 (2016).
43. J. Cerezo, I. Vandendael, R. Posner, J. H. W. de Wit, J. M. C. Mol, and H. Terryn, *Appl. Surf. Sci.*, **366**, 339 (2016).
44. I. Schoukens, I. Vandendael, J. De Strycker, A. A. Saleh, H. Terryn, and I. De Graeve, *Surf. Coat. Technol.*, **235**, 628 (2013).
45. L. Li, A. L. Desouza, and G. M. Swain, *Analyst*, **138**, 4398 (2013).
46. L. Li, B. W. Whitman, and G. M. Swain, *J. Electrochem. Soc.*, **162**, C279 (2015).
47. L. I. Fockaert, P. Taheri, S. T. Abrahami, B. Boelen, H. Terryn, and J. M. C. Mol, *Appl. Surf. Sci.*, **423**, 817 (2017).
48. N. W. Khun, G. S. Frankel, and J. Zimmerman, *Corrosion*, **69**, 259 (2012).
49. S. Verdier, S. Delalande, N. van der Laak, J. Metson, and F. Dalard, *Surf. Interface Anal.*, **37**, 509 (2005).
50. S. Verdier, N. van der Laak, F. Dalard, J. Metson, and S. Delalande, *Surf. Coat. Technol.*, **200**, 2955 (2006).
51. P. Taheri, K. Lill, J. H. W. de Wit, J. M. C. Mol, and H. Terryn, *The Journal of Physical Chemistry C*, **116**, 8426 (2012).
52. P. Taheri, P. Laha, H. Terryn, and J. M. C. Mol, *Appl. Surf. Sci.*, **356**, 837 (2015).
53. T. Lostak, A. Maljusch, B. Klink, S. Krebs, M. Kimpel, J. Flock, S. Schulz, and W. Schuhmann, *Electrochim. Acta*, **137**, 65 (2014).
54. T. Lostak, S. Krebs, A. Maljusch, T. Gothe, M. Giza, M. Kimpel, J. Flock, and S. Schulz, *Electrochim. Acta*, **112**, 14 (2013).
55. R. Mohammad Hosseini, A. A. Sarabi, H. Eivaz Mohammadloo, and M. Sarayloo, *Surf. Coat. Technol.*, **258**, 437 (2014).
56. H. E. Mohammadloo, A. A. Sarabi, A. A. S. Alvani, R. Salimi, and H. Sameie, *Mater. Corros.*, **64**, 535 (2013).
57. H. E. Mohammadloo, A. A. Sarabi, R. Mohammad Hosseini, M. Sarayloo, H. Sameie, and R. Salimi, *Prog. Org. Coat.*, **77**, 322 (2014).
58. N. W. Khun and G. S. Frankel, *Mater. Corros.*, **66**, 1215 (2015).
59. N. W. Khun and G. S. Frankel, *Corrosion*, **71**, 277 (2014).
60. X. Liu et al., *ACS Applied Nano Materials*, **2**, 1920 (2019).
61. S. Adhikari, K. A. Unocic, Y. Zhai, G. S. Frankel, J. Zimmerman, and W. Fristad, *Electrochim. Acta*, **56**, 1912 (2011).
62. H. R. Asemani, P. Ahmadi, A. A. Sarabi, and H. Eivaz Mohammadloo, *Prog. Org. Coat.*, **94**, 18 (2016).
63. O. Lunder, F. Lapique, B. Johnsen, and K. Nisancioglu, *Int. J. Adhes. Adhes.*, **24**, 107 (2004).
64. M. Sababi, H. Terryn, and J. M. C. Mol, *Prog. Org. Coat.*, **105**, 29 (2017).
65. W. Zhu, W. Li, S. Mu, N. Fu, and Z. Liao, *Appl. Surf. Sci.*, **405**, 157 (2017).
66. Y. Liu, G. Z. Meng, and Y. F. Cheng, *Electrochim. Acta*, **54**, 4155 (2009).
67. Y. Liu and Y. F. Cheng, *J. Appl. Electrochem.*, **41**, 151 (2011).
68. M. Zamin, *Corrosion*, **37**, 627 (1981).
69. M. A. Smit, J. M. Sykes, J. A. Hunter, J. D. B. Sharman, and G. M. Scamans, *Surf. Eng.*, **15**, 407 (1999).
70. M. A. Smit, J. A. Hunter, J. D. B. Sharman, G. M. Scamans, and J. M. Sykes, *Corros. Sci.*, **46**, 1713 (2004).
71. E. P. Banczek, S. R. Moraes, S. L. Assis, I. Costa, and A. J. Motheo, *Mater. Corros.*, **64**, 199 (2013).
72. M. Mujdrica Kim, B. Kapun, U. Tiringer, G. Šekularac, and I. Milošev, *Coatings*, **9**, 563 (2019).

73. R. G. Kelly, J. R. Scully, D. W. Shoesmith, and R. G. Buchheit, in *Electrochemical Techniques in Corrosion Science and Engineering* (Marcel Dekker, Inc., New York-Basel) p. 440 (2003).
74. ASTM International, G 59–97, Standard Test Method for Conducting Potentiodynamic Polarization Resistance Measurments, ASTM International, West Conshohocken, PA, United States of America (2014).
75. H. Eivaz Mohammadloo, A. A. Sarabi, A. A. Sabbagh Alvani, H. Sameie, and R. Salimi, *Surf. Coat. Technol.*, **206**, 4132 (2012).
76. X. Chen, G. Li, J. Lian, and Q. Jiang, *Surf. Coat. Technol.*, **204**, 736 (2009).
77. B. Szczygieł, J. Winiarski, and W. Tylus, *Mater. Chem. Phys.*, **129**, 1126 (2011).
78. E. M. Fayyad, M. A. Almaadeed, A. Jones, and A. M. Abdullah, *Int. J. Electrochem. Sci.*, **9**, 4989 (2014).
79. N. Birbilis and R. G. Buchheit, *J. Electrochem. Soc.*, **152**, B140 (2005).
80. N. Birbilis, R. G. Buchheit, and M. K. Cavanaugh, *ECS Trans.*, **1**, 115 (2006).
81. S. D. Scully Jr and M. W. Kendig, in *Electrochemical Impedance: Analysis and Interpretation* (ASTM International, Philadelphia, USA) (1993).
82. F. Mansfeld, in *Analytical Methods in Corrosion Science and Engineering*, ed. F. B. M. Philippe Marcus (CRC Press, Taylor & Francis Group, Boca Raton) 1st ed., p. 463 (2005).
83. F. Mansfeld, *Electrochim. Acta*, **35**, 1533 (1990).
84. R. G. Kelly, J. R. Scully, D. W. Shoesmith, and R. G. Buchheit, in *Electrochemical Techniques in Corrosion Science and Engineering* (Marcel Dekker, Inc., New York-Basel) p. 440 (2002).
85. R. G. Buchheit, M. Cunningham, H. Jensen, M. W. Kendig, and M. A. Martinez, *Corrosion*, **54**, 61 (1998).
86. Y. J. Li and L. Arnberg, *Mater. Sci. Eng.*, **347**, 130 (2003).
87. L. F. Mondolfo, in *Aluminum Alloys: Structure and Properties* (Butterworth & Co Ltd., London; Boston) p. 1277 (1976).
88. J. van den Brand, W. G. Sloof, H. Terryn, and J. H. W. de Wit, *Surf. Interface Anal.*, **36**, 81 (2004).
89. E. McCafferty and J. P. Wightman, *Surf. Interface Anal.*, **26**, 549 (1998).
90. I. Milošev, H. H. Strehblow, and B. Navinšek, *Surf. Interface Anal.*, **26**, 242 (1998).
91. X. Dou, D. Mohan, C. U. Pittman Jr, and S. Yang, *Chem. Eng. J.*, **198**, 236 (2012).
92. M. A. L. Braulio, M. Rigaud, A. Buhr, C. Parr, and V. C. Pandolfelli, *Ceram. Int.*, **37**, 1705 (2011).
93. A. Goldstein, *J. Eur. Ceram. Soc.*, **32**, 2869 (2012).